



Report on the feasibility of GFR fuel for minor actinide management

Revision No: 0
Effective Date: 30-Aug-2004

Prepared by: M. K. Meyer

Title: Report on feasibility of GFR fuel for minor actinide management

Author: M. K. Meyer

Revision No: 0

Effective Date: 30-Aug-2004

Abstract: In large part, the feasibility of the GFR for minor actinide burning depends upon the limitations inherent to the fuel. GFR fuel concepts represent a compromise between heavy metal density and the ability to withstand GFR severe accident conditions. Since no data exists on the irradiation behavior of proposed GFR fuels under GFR core operating conditions, the assessments in this report are made on the basis of scoping analysis of fuel concepts. A combination of behavior correlations and finite element analysis were used to make relative judgments about the impact of minor actinide loading on fuel burnup lifetime. It appears from literature data that the primary factor distinguishing MA-bearing fuel behavior is the generation of large additional inventories of helium gas due to capture and decay processes beginning with ^{241}Am . This large gas inventory is problematic for the GFR, where loss of core pressurization results both in a rapid temperature rise and the removal gas overpressure that acts as a restraining force.

In general, pin-type fuel is most adaptable to the issues posed by burning minor actinides. Fuel to plenum volume ratios can be adjusted to account for the increased gas inventory at the cost of increased pressure drop and a larger volume required for the core primary pressure vessel. Creep strengths of refractory metal cladding materials are quite low at GFR accident temperatures and conventional sealed pin-type fuels would require a very large plenum, on the order of 2-3X the fuel volume, to accommodate the gas release at an americium loading of 10 at.% of the heavy metal at 10 at.% burnup. An alternative to sealed pin-type fuel may be vented fuel or fuel fitted with a rupture disk system. In this case, considering only gas-loading of the cladding as the life-limiting factor for the fuel, the potential for MA loading is much higher, and there are no requirements for a long gas plenum.

Because particle packing density is low in a particle bed fuel and all fission gas must be accommodated internally in a 'buffer layer' (effectively a gas plenum), fuel particle coating layers must be very thin relative to those used on TRISO fuel. As a result, high stresses are generated in the fuel particle shell wall under core accident conditions even for fuels containing no americium. Particle bed fuels thus have marginal utility for MA management.

Coated particles dispersed in a solid matrix offer more restraint to particle swelling. Because of the nature of dispersion fuel, the 'gas plenum' is integral to the fuel particle. Increase in 'gas plenum' volume always result in lower heavy metal density in the fuel. This is in contrast to pin-type fuels, where increasing the gas plenum length has no impact on the heavy metal density within the GFR active core volume. Dispersion fuel thus offers less flexibility than pin-type fuel for burning minor actinides whose primary fuel performance attribute is the generation of additional gas inventory. Dispersion fuel models indicate a significant increase in matrix stress at americium levels above approximately 5 at.% during core accident conditions, where temperatures are assumed to be reach 1600°C. At 5 at.% Am content, it is speculated that fuel burnup limits would be reduced by 15-20% relative to fuel that contains no americium. Dispersion fuel is thus considered a viable concept for managing minor actinides at levels on the order of 5 at.% heavy metal or less.

Due to the extremely complex nature of fuel behavior under irradiation, fuel irradiation testing is necessary for final determination of viability; without irradiation test data, no concrete statements about viability can be made. This is especially true for the GFR, where operating parameters and fuel physical requirements are outside of the envelope of the current experimental fuel database.

1.0 INTRODUCTION

This report gauges the feasibility of minor actinide (MA) management using the Generation IV Gas-cooled Fast Reactor (GFR) concept from the perspective of fuel irradiation behavior.

Fast spectrum gas-cooled system concepts are designed to operate at much higher power density and have much smaller core heat capacitance than thermal spectrum gas-cooled systems. Typical core power densities for gas-cooled thermal spectrum reactor systems are in the neighborhood of 6 MW/m^3 , while current designs for GFR systems call for values in the range of $50\text{-}100 \text{ MW/m}^3$. Current (thermal spectrum) high-temperature gas reactor designs rely on the use of coated fissile particles widely dispersed in massive graphite blocks, in contrast to the high fuel heavy metal density required for the GFR. The large mass of graphite in thermal spectrum gas-cooled reactors provides for heat transfer and thermal inertia, resulting in slow thermal transients on loss of coolant. TRISO (tri-layer coated particle) fuel, used in thermal spectrum reactors, is not adaptable to a gas-cooled fast reactor, however, due to low fissile loading, the swelling behavior of graphite in a fast spectrum, and excessive moderation due to the large graphite/fuel ratio.

The neutronic requirements of a fast spectrum converter (low parasitic absorption), the need for high fissile atom density to maintain a conversion ratio of unity, and the requirement for fission product containment at high temperature (to allow the use of direct cycle power generation) greatly reduce the field of fuel types that can be realistically considered for GFR application. The current state of the art for GFR fuel consists of a number of fuel concepts and estimates of viability based on identification of potential life-limiting factors and order-of-magnitude modeling of the effects of these factors on fuel temperature capability and burnup potential.

The assessments in this report on the feasibility of using GFR fuel for MA burning are made on the basis of scoping analysis of fuel concepts; little experimental data is available to support these assessments. Calculations are made on the basis of the reference helium-cooled direct cycle variant of the GFR concept with parameters as listed in Table 1.1. Some further incremental progress on determining the viability of minor actinide transmutation using GFR fuel concepts can be made by developing more sophisticated fuel performance models; this requires that a well defined set of material properties and irradiation performance correlations be available for use by fuel designers and modelers. In addition, analysis of the potential effects of the shift in fission product distribution on internal fuel chemistry can be more clearly defined, as well as potential decreases in fuel thermal conductivity. In the end, due to the extremely complex nature of fuel behavior under irradiation, fuel irradiation testing is necessary for final determination of viability; without irradiation test data, no concrete statements about viability can be made. This is especially true for the GFR, where operating parameters and fuel physical requirements are outside of the envelope of the current experimental fuel database.

Table 1.1. GFR Reference Design Parameters

System Parameter	Reference Value
Power level	600 MWth
Net efficiency	48%
Coolant pressure	70 bar
Outlet coolant temperature	850 °C
Inlet coolant temperature	490 °C
Nominal flow & velocity	330 kg/s & 40 m/s
Core volume	5.8 – 10.7 m ³
Core pressure drop	~0.4 bar
Volume fractions of Fuel/Gas/SiC	50/40/10 %
Average power density	50 - 100 MW/m ³
Reference fuel composition	UPuC/SiC (50/50 %)
Breeding/Burning performances	fissile breakeven
In core heavy metal inventory	8-15 MT
Fissile (TRU) enrichment	~20 wt%
Fuel management	multi-recycling
Fuel residence time	3 × 829 efpd
Discharge burnup ; damage	~10 at%
Primary vessel diameter	<7 m

2.0 GENERAL ASSESSMENT OF GFR FUEL CONCEPTS

2.1 Screening criteria for GFR fuel concepts

There are no currently developed fuels that meet all GFR requirements. Initial screening criteria for new fuels were selected on the basis of satisfying GFR specific requirements developed on the basis of the Generation IV goals of sustainability, economics, proliferation resistance, and safety/reliability. GFR specific fuel attributes linked to these goals are listed in Table 2.1

Table 2.1. Gen IV goals and impact on GFR fuel requirements.

Gen IV Goal	GFR Fuel Attributes
Sustainability	1(a) High heavy metal density to allow for self-breeding 1(b) Fuel suitable for use in closed fuel cycle 1(c) Fuel performance must be compatible with full actinide recycle 1(d) Fuel must be compatible with remote fabrication
Economics	2(a) High burnup 2(b) Reasonable recycle cost
Proliferation resistance	3(a) No separation of minor actinides, all minor actinides incorporated into fuel 3(b) No breeding blanket requires higher in-core heavy metal density
Safety/Reliability	4(a) No core restructuring during any accident scenario 4(b) Direct cycle power conversion requires low fission product release

Based on Generation IV goals and the GFR fuel attributes derived from them, a simple set of criteria with a common basis among all fuels was selected for initial screening of fuel types; these criteria are listed in Table 2.2. More comprehensive requirements were developed for specific fuel types based on the results of core neutronic and thermohydraulic studies.

Table 2.2 GFR initial fuel screening criteria.

Screening Criteria	Defining Requirement	Reference Value used for Screening
Melting temperature	4(a)	> 2000°C
Fuel heavy metal density	1(a), 3(a), 3(b)	> 5 g/cm ³
Fuel burnup potential	2(a)	5-10 at.% HM

The fuel temperature requirement, derived from the goal to exclude melting under unprotected loss of flow conditions is the most limiting in terms of fuel selection, and when coupled with core neutronic requirements, severely limits the range of possible fuels. Obviously, current fuels such as zirconium-clad LWR fuel and stainless steel clad fast reactor fuels are excluded on the basis of cladding melting temperature. TRISO

coated particle fuel is excluded on the basis of low heavy metal density. Burnup potential of fuels is somewhat more difficult to gauge, but does not appear to be overly restrictive.

Many fuel types can be eliminated out of hand; a few require more careful consideration. Two categories of fuel have the highest potential for success; carbide and nitride-based composite-type (dispersion) fuels and pin-type refractory ceramic fuel. Many variants of pin-type fuels have been extensively developed, and offer a large database on which to base estimates of fuel performance (although there are still sizable gaps). This fuel type currently has limitations in high temperature performance due to the lack of a suitable refractory cladding material. Breakthroughs in cladding development, such as the successful development of SiC composite cladding material may make this fuel type acceptable for GFR use. Pin-type fuel based on ODS steels (Oxide Dispersion Strengthened) may be used for a GFR demonstration core startup. Duplex-type cladding materials, consisting of a SiC fiber composite shell encasing an alloy cladding tube may also be possible, and would likely meet the criteria of 'no core restructuring' while still allowing seal welds to be made by more-or-less conventional fusion welding technology. Another possibility is the use of vented cladding tubes.

Dispersion fuels (also referred to as composite fuels) offer the potential to reach goal burnup and offer a larger range of flexibility in the choice of materials. These fuels consist of a distribution of discrete fuel particles embedded in a refractory matrix. The concept most likely to be successful for composite fuel will use thinly coated particles (or elongated elliptical 'rods') embedded in an inert matrix. In the ideal case, the matrix remains largely unaffected by neutron, fission fragment, and α -particle damage from the fission events that take place in the fuel particles. Although this fuel type appears best suited to withstand the high temperatures possible in GFR unprotected loss-of-coolant accidents, it has limitations in terms of heavy metal density.

In addition, initial screening identified particle bed assemblies as a potential fuel type meeting GFR goals, although the resolution of many technical issues remains uncertain. This fuel type has been selected as the front-runner for the current Japanese GFR concept.

Two fuel types, pin-type fuels and dispersion fuels, were thus selected for detailed further study. Also considered to a lesser degree were particle bed fuels. In the following sections, reference fuel designs are proposed for pin-type and dispersion fuels. The primary factors that differentiate fuels for minor actinide burning are assessed, and assessments of the applicability of these fuels to burning minor actinides are made for on the basis of fuel behavior models and available material property data.

2.2 Pin-type fuel

2.2.1 Overview and Requirements

Pin type fuel is attractive due to the large operating database accumulated for similar fast reactor fuels and cladding materials. The high outlet temperature of the GFR and the requirement for exclusion of core restructuring as a result of clad melting, however, eliminates all steel-based alloys, including ODS (Oxide Dispersion Strengthened) steels, from consideration.

Fuel response to the core conditions following a loss-of-coolant event is the overriding factor in the design of pin-type fuels. A gas plenum must be built into the fuel to accommodate gas release. During normal reactor operation at 70 bar coolant pressure, fuel can be designed such that the net stress on the cladding is compressive; the coolant pressure is larger than the pin internal pressure. The plenum length is then a compromise between internal gas pressure that can be tolerated during core depressurization and shutdown and the coolant pressure drop through the core during operation.

During an unprotected LOCA, however, core coolant pressure decreases coincident with both core and fuel temperature increases. This increase in fuel temperature causes increased fuel pin internal pressure due to both gas pressurization and an increased gas release rate from the fuel. This increase in pin internal pressure, coupled with the lack of external core pressure causes a large increase in cladding tensile hoop stress. This increase in cladding tensile hoop stress occurs coincident with a decrease in cladding creep strength due to the cladding temperature increase. This combination of events during unprotected LOCA, coupled with core design constraints driven by plenum height restrictions make conventional sealed pin design for GFR fuel difficult to implement.

Alternatives to sealed fuel pin designs that alleviate the above problem due to pressure and temperature excursions during LOCA include a common plenum in the low temperature region of the core, fuel pins containing rupture disks that allow pin depressurization to the coolant prior to ballooning, or vented fuel pins.

Specific requirements for pin-type fuel are, in general, similar to those defined for liquid metal-cooled fast reactors and are listed in Table 2.3, except that the required cladding melting temperature is much higher.

Table 2.3 Pin-type Fuel Requirements

Requirement	Reference Value
Maximum Diametral Swelling	<2%
Peak Dose	> 80 dpa
Clad Melting Temperature	>2000°C

2.2.2 Fissile Phase Considerations

Two primary factors are involved in the selection of the fissile phase for pin-type fuel; these are core neutronic and fuel performance. Core neutronics calculations performed as a result of the U.S./French INERI program indicate that oxide fuel is a poor performer from the perspective of core neutronics relative to carbide and nitride fuels due to low heavy metal density and spectral softening due to the presences of oxygen. Excluding oxide fuel, the primary choices of fissile phase become mixed carbide and nitride fuels. Both fuels have been demonstrated to perform well to burnups on the order of 8-12% HM in sodium cooled fast reactor systems. These systems operate at lower cladding temperatures but higher power densities relative to current GFR requirements.

There are no outstanding considerations related to fuel behavior that separate carbide and nitride fuels. Scoping fuel performance analyses do not differentiate these fuels at a generic level. At lower burnup, mixed nitride fuel swelling and gas release tends to be lower than that of carbide fuel. As burnup increases, however, these differences in gas release and swelling behavior decrease. Considerably more fuel performance data is available for mixed carbide fuels, including swelling and gas release correlations, although much of the data is for fuels with high oxygen content, which tend to exhibit higher swelling. Data is also available for carbide sphere-pac fuel.

Another consideration is the need for ^{15}N enrichment and recycle for nitride fuel for reasons of neutron economy in the GFR system. The presence of ^{14}N strongly affects core breeding performance. The order of magnitude to which this additional expense effects fuel cycle cost are a source of significant uncertainty which favor the use of carbide fuel.

It is likely that the overriding factor in fissile phase (pellet) selection for a pin-type concept will be driven by cladding compatibility, a fuel performance consideration.

2.2.3 Cladding Selection

The goal to prevent core restructuring coupled with core neutronic requirements limits the potential choice of cladding materials. Alloy base-metals and metalloids that meet the 2000°C melting temperature requirement are B, C, Nb, Mo, Ru, Hf, Ta, W, Re, Os, and Ir. It is obvious that B and Hf are not practical materials for this application due to their effect on core neutron economy and that Ru, Os, and Ir are not practical due to cost and availability. Scoping core neutronics studies have also shown that cores clad with Ta, W, and Mo require very large heavy metal inventories to allow self breeding. Carbon and carbon/carbon composites have a service life of less than 15 dpa [1], compared to the $\gg 100$ dpa required during the service life of fuel at 100 % burnup, and are also excluded.

The remaining allowable alloy base metal, Nb, was developed in alloy form as Nb-1Zr and PWC-11 (Nb-1Zr-0.06C) during the SP-100 space reactor program. Many fuel irradiation experiments have been conducted using variants of Nb-Zr cladding and UN

fuel to burnups of approximately 6% in fast spectrum environments. [2] A thin rhenium cladding inner liner was found to be important for limiting fuel-cladding-chemical-interaction. Neutronic performance of Nb-1Zr clad fuel encased in Nb-1Zr ducts is marginal for the GFR, but improves when SiC is used as the duct material. [3] Concerns related to the use of Nb-based alloys are performance in case of air ingress associated with high core temperatures during a LOCA and sensitivity to coolant impurities. In the case of air ingress at high temperature, the cladding would be heavily oxidized and may lose structural integrity and allow fuel movement. Careful control would also have to be exercised over reactor coolant impurity content during normal operation. A potential alternative includes the use of Nb-1Zr based materials as a potential inner shell in a duplex cladding system, where the outer shell is designed to protect the alloy from interaction with the coolant.

SiC is another potential cladding choice, although at a much earlier stage of development. Joining of SiC to SiC or other materials is a major issue confronting development of SiC cladding. A method for cladding development that appears promising is the NITE (Nano Infiltration Transient Eutectic) process developed in Japan at Kyoto University, although little detailed information has been published in the open literature in the English language. Work on joining SiC has also been conducted as a part of this program.

Other potential processes include CVI (Chemical Vapor Infiltration) of a fiber preform woven over a monolithic SiC tube being conducted under a DOE SBIR (Small Business Innovative Research) grant by Gamma Engineering. [4] A SiC reinforced ferritic steel cladding is also under development [5]. The best near-term approach may be the hybrid approach, where a metallic liner is used to ensure a hermetic seal and ease pin closure issues.

SiC cladding is most compatible with mixed carbide fuel. Reaction of SiC with UN is thermodynamically favorable above 550°C, although reaction could presumably be prevented through the use of a cladding liner. SiC composites have demonstrated good irradiation behavior [6] and should be capable of maintaining mechanical properties at dose levels well beyond 50 dpa at temperatures of less than 1000°C.

2.2.4 Reference and Alternate Concepts

Significant unknowns confronting the development of SiC cladding and the integral performance of SiC clad mixed carbide fuel must be weighed against the more developed but less suitable Nb-1Zr clad nitride fuel. Nb-1Zr has the additional difficulties of requiring tight control of coolant impurity level, particularly oxygen and hydrogen; SiC is more robust in this regard. Nb-based cladding materials may have to be protected from interaction with coolant impurities by a protective outer shell. (U,Pu)N fuel, most compatible with Nb-1Zr cladding, requires enrichment in ¹⁵N for neutronic reasons, which represents a significant unknown in terms of fuel cycle cost. In view of these tradeoffs and the relatively unknown state of technology, neither technology offers a definite advantage.

SiC clad (U,Pu)C fuel is selected as the reference for pin-type fuel, however, in light of the potential of this fuel system in meeting Gen IV goals. SiC offers improved core neutronic performance over Nb alloys and expected robust behavior in the case of air ingress into the core during accident events. In addition, this fuel combination has the advantage of not requiring the production and recycle of enriched nitrogen. Significant difficulties relating to the manufacture and sealing of thin-walled composite tubes also need to be resolved.

2.3 Particle bed fuel

2.3.1 Overview

Coated particle fuels (CPF) configured as a particle bed or as a fluidized bed have been considered primarily for nuclear propulsion applications in the past, [7,8,9] but have also received cursory consideration for use as a reactor system for minor actinide burning [10]. The primary advantages in using such a system are the low thermal gradients across each fuel unit (particle) and a high heat transfer area, resulting in low thermal stresses within fuel particles and the ability to resist fuel damage during transients. The primary issues with such a system are related to practical matters in fuel element design, particularly the design of a reliable frit material to keep fuel particles from exiting the reactor and preventing the possibility of frit clogging under conditions in which fuel particles generate aerosols or small fragments due to failure. Pressure drop across assemblies also tends to be higher than for fuel designs with discrete channels, although this can be offset by using thin beds, within the constraints imposed by heavy metal loading requirements in the core.

2.3.2 Fuel Design

Detailed fuel design studies have not been conducted in the U.S. The Japanese have adopted a particle bed core as the reference for the GFR under their ongoing 'feasibility study'. The Japanese core consists of horizontal flow assemblies, as depicted in Figure 2.1 (b) [11]. Particles consist of a TiN porous buffer and seal coat of TiN over large diameter (U,Pu)N particles Fig 2.1 (a). The frit material is a SiC composite, as are the other structural components. Similar particle bed designs have been studied by the French CEA [12]. An alternate design (Fig 2.1(c)), consisting of a bed of particles embedded in a solid SiC matrix is also considered; this is equivalent to a ceramic matrix dispersion fuel.

Significant concerns regarding this concept relate to fuel particle integrity, performance, and retention in the subassembly. The failure behavior of ceramics is controlled by the presence of microstructural defects introduced primarily during fabrication; failure is induced by stress concentrations around these defects leading to crack growth. A net compressive stress field does not lead to crack propagation, thus ceramics are considerably stronger in compression than tension. During normal core operation, a net compressive stress is imposed by core coolant pressure. During loss-of-coolant scenarios, this force is removed. In TRISO fuel designs, the SiC 'pressure vessel' layer

relies on irradiation-induced shrinkage of the inner and outer pyrocarbon layers in order to maintain a net compressive stress in the coating until late in its service life. The absence of the two pyrocarbon coating layers allows a net tensile stress to develop in the coating as a result of fission gas pressurization, and will almost certainly lead to a much less robust fuel. Because strength in ceramics is flaw controlled, statistical data from materials produced by prototypic fuel particle fabrication methods is required in order to estimate particle failure probability. This concern is offset to some degree by embedding the particles in a solid matrix, where manipulation of the relative thermal expansion coefficients can lead to a net compressive stress in the particle coating during operation. This is a dispersion fuel concept.

A second concern that has not been addressed for particle bed concepts is the affect of particle-to-particle movement on fuel behavior. The particle bed is similar in design to vibratory mills, which provide effective means of reducing particle size in the ceramic industry, thus care must be taken to avoid the possibility of excessive particle motion within the bed during reactor operation. Finally, the effect of interparticle sintering or fusion on subassembly flow and particle failure must be addressed. Given these concerns, the particle bed assembly, offers greater uncertainties and obstacles to development than either of the other two concepts considered.

2.3.3 Reference Concept

No distinct U.S. reference is suggested for the particle bed fuel concept. Given the early state of development of this concept, both the CEA or Japanese designs are considered equivalent.

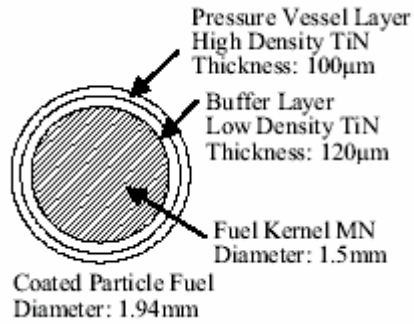


Figure 2.1 (a). Japanese coated particle concept for particle bed GFR.

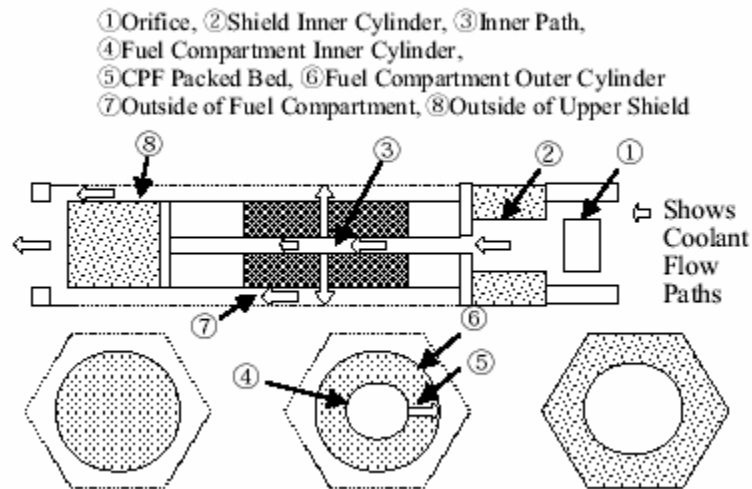


Figure 2.1(b). Japanese horizontal flow particle bed subassembly.

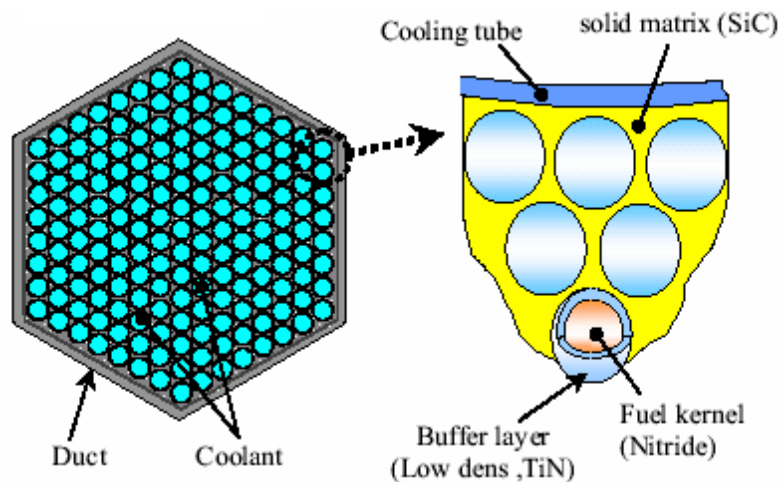


Figure 2.1 (c). Japanese 'solid matrix' coated particle fuel subassembly design.

2.4 Dispersion fuel

2.4.1 Overview

Dispersion fuels (also referred to as composite fuels) offer the potential to reach goal burnup and offer more flexibility in choice of materials than pin-type concepts. These fuels consist of a distribution of discrete fuel particles embedded in a non-fuel matrix.

Dispersion fuels have been shown to be capable of very high burnup, in certain cases far exceeding the ATW goal burnup of 30%. Properly fabricated UO₂ dispersions in stainless steel have been shown to be capable of ²³⁵U burnup >70% at 93% enrichment. This experience is not directly applicable to an americium-bearing fuel, however, because of additional stress exerted on the matrix by helium gas production.

Dispersion fuels are heterogeneous mixtures of fuel particles dispersed in a matrix material that provides mechanical restraint and an efficient path for heat conduction away from the fuel [13] An ideal dispersion consists of spherical particles uniformly distributed throughout a chemically and neutronically inert matrix material. In order to minimize the total matrix volume damaged by fission fragment recoil from the fuel particles and retain matrix strength, fuel particles should be large compared to the fission fragment range in the matrix, and the fuel particle volume fraction should be low enough to ensure that damage zones do not overlap. [14] Dispersion fuel performance is thus sensitive to fabrication parameters, microstructure, and matrix strength at temperature.

Composite fuel performance depends heavily on the microstructural characteristics of the fuel. Two primary strategies have been pursued for optimizing fuel behavior through manipulation of microstructural variables. Macrodispersions attempt to maintain the thermal conductivity and structural integrity of the matrix during irradiation through the use of relatively large and widely distributed fissile phase particles. Microdispersions incorporate a fine dispersion of the fissile phase into a neutronically inert matrix. This is often done as a convenience for fabrication. In the case of a microdispersion, fission related damage occurs over a larger fraction of the matrix volume relative to a macrodispersion, introducing the possibility for fission fragment driven matrix swelling. Macrodispersions are thus preferred for the composite-type fuel currently envisioned for the GFR. In the ideal case, the matrix remains largely unaffected by neutron, fission fragment, and α -particle damage from the fission events that take place in the fuel particles. The concept most likely to be successful for composite fuel will use thinly coated particles (or elongated elliptical ‘rods’) embedded in an inert matrix.

2.4.2 Dispersion Fuel Particle Concepts

Two types of fuel particle designs have been considered for GFR dispersion fuels. These are particles fabricated with and without a buffer layer.

The simplest dispersion fuel concept, and the one with the highest potential fuel loading, consists simply of a (non-buffered) fuel particle embedded in an inert matrix. This

particle may incorporate a thin barrier coating to prevent fuel/matrix chemical interaction from occurring during fabrication and irradiation. Such particles typically include a distribution of approximately 15% open porosity to act as a fission gas ‘plenum’ reducing the gas-driven pressure on the matrix. Dispersions using this concept have been proven to work well in combination with ductile matrices such as steel [15] and niobium [16]. Figure 2.2 (a) shows a schematic drawing of this fuel type. Figure 2.2 (b) shows, as an example, a dispersion of oxide fuel in a stainless steel matrix. This combination of ductile matrix and ‘unbuffered’ fuel particle has been proven to be quite robust in numerous irradiation tests of metallic matrix fuels. Performance has been empirically postulated to be limited by a combination of fission density and temperature. Fuel fission density is linked both to fuel particle loading and burnup. Figure 2.2 (c) shows a plot of irradiation data for plate-type dispersion fuels circa. 1963 [17]. Fuels lying to the left of the line are postulated to be stable; those to the right, unstable during irradiation. Note that the ‘stability line’ will likely be shifted further to the right for dispersion fuel configurations such as blocks and plates, due to a more favorable distribution of stress in these cases.

The ‘unbuffered’ fuel concept works well when used with ductile matrix materials, however experiments in dispersion fuels fabricated with particles directly in contact with ceramic matrices produce less favorable results. Several irradiation tests have been conducted using oxide-based cermet fuel concepts in France [18,19] and Japan [20]. Matrix cracking has been observed in all of these cases, leading to higher than expected fission gas release. This behavior has been attributed to stresses imposed on the matrix both from fuel particle swelling and the differences in thermal expansion coefficient between the fuel particles and the matrix. Also examined in the THERMHET irradiation test in France was the so-called ‘jingle’ variant of the macrodispersed concept, which incorporates free space between the fuel particle and matrix. This concept shows promise in reducing matrix fracture due to fuel/matrix mechanical interaction, although some matrix cracking was still observed. [21]

Figure 2.3 (a) shows the results of a finite element calculation of the maximum principal stress induced by thermal expansion mismatch in a composite consisting of UC particles dispersed and bonded to a SiC matrix; here the stress free temperature is 25 °C. It can be seen that at 1000°C, a maximum principal stress >360 MPa occurs due to thermal expansion mismatch alone. This stress level will be unacceptable for ceramic materials, which do not readily deform and relax these stresses. (In reality, the stress free temperature will be approximately the fabrication temperature, resulting in a somewhat different stress distribution in the matrix).

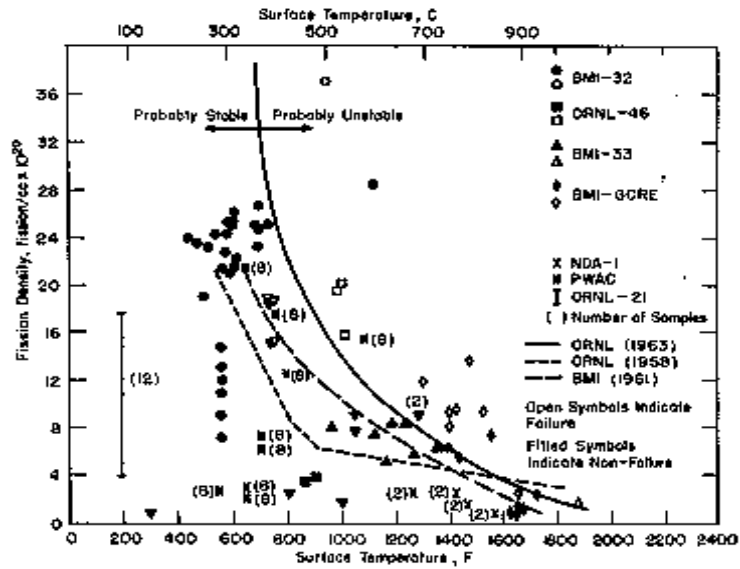
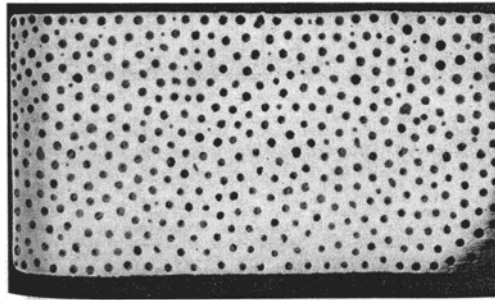
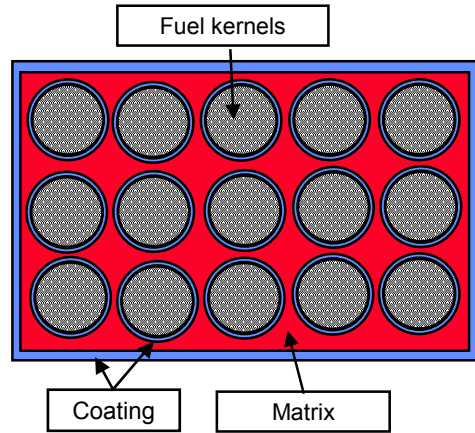


Figure 2.2. (a) Schematic on 'unbuffered' dispersion fuel. (b) Example of dispersion of UO_2 in stainless steel. (c) Plot of fission density vs. surface temperature showing empirical regimes of stability for UO_2 dispersions in stainless steel.

Given the available cermet irradiation behavior database, the concept most likely to minimize fission gas release to the coolant will incorporate 'buffered' particles in a dense matrix. This concept is shown in Figure 2.3 (b). Here each particle is surrounded by a low density layer of material with low crush strength. This 'buffer' material serves the dual role of providing volume for fission gas and providing volume for fuel particle swelling. The buffer layer is protected by a dense layer, also designed to provide for fission product retention. In this way, there are three barriers to fission product release to the coolant. These are the coating around the particle, the dense matrix, and the cladding around the fuel block.

The use of coated particles makes it more difficult to achieve high heavy metal density in the fuel. Since fuel particle volume increases in proportion to the cube of the particle radius, the net heavy metal density within a fuel particle falls rapidly with increasing coating thickness. This fact requires that the coating thickness to kernel diameter ratio be kept as small as possible while maintaining utility as a fission product barrier. Shown in Figure 2.3 (c) is a plot of matrix stress in a free particle due to fission gas release plotted over the ratio of coating thickness to kernel diameter for a fixed buffer layer thickness at 10% burnup. The buffer layer thickness was chosen accommodate 15 volume percent fuel particle swelling. This plot is, of, course, the result of specific assumptions about the fission gas release rate from the fuel kernel. From the plot, it can be seen that below a ratio of 0.1 at 1473 K, the stress in the coating outer shell increases rapidly with decreasing coating thickness. The coating thickness to kernel diameter ratio should thus be maintained at 0.1 or slightly greater. In order to eliminate local stresses due to differential thermal expansion, the thermal expansion coefficients of the fuel particle coating and the matrix should be matched.

The most likely fissile particle types for composite fuels are (U,Pu)C and (U,Pu)N, due the combination of high melting temperature and high actinide density. Although a dispersion of nitride fuel particles may exhibit lower fission gas release than the carbides, the same questions related to the use of ^{15}N in the fuel matrix apply to nitride fuel particles. Chemical compatibility issues favor the use of a nitride coating system (TiN, ZrN) for mixed nitride kernels and a carbide coating system (SiC, ZrC) for mixed carbide kernels. Because of the poor irradiation performance of pyrocarbon at high fast fluence, the use of a low density pyrocarbon buffer layer is questionable. Low density carbide and nitride coatings with low crush strength deposited from non-halide precursors may be more suitable.

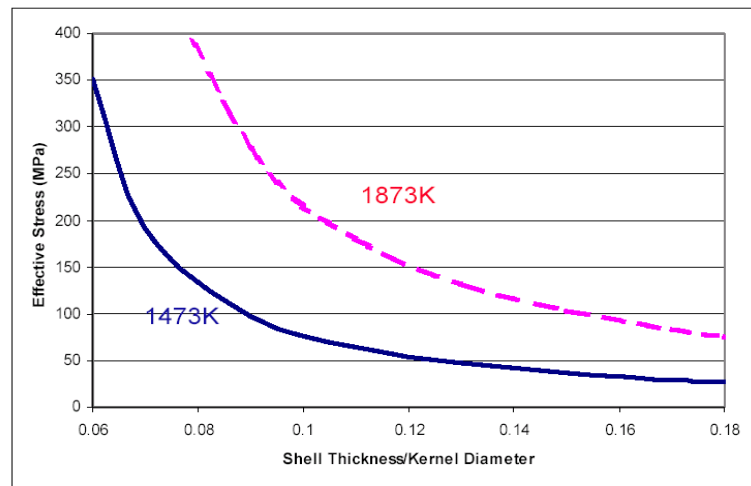
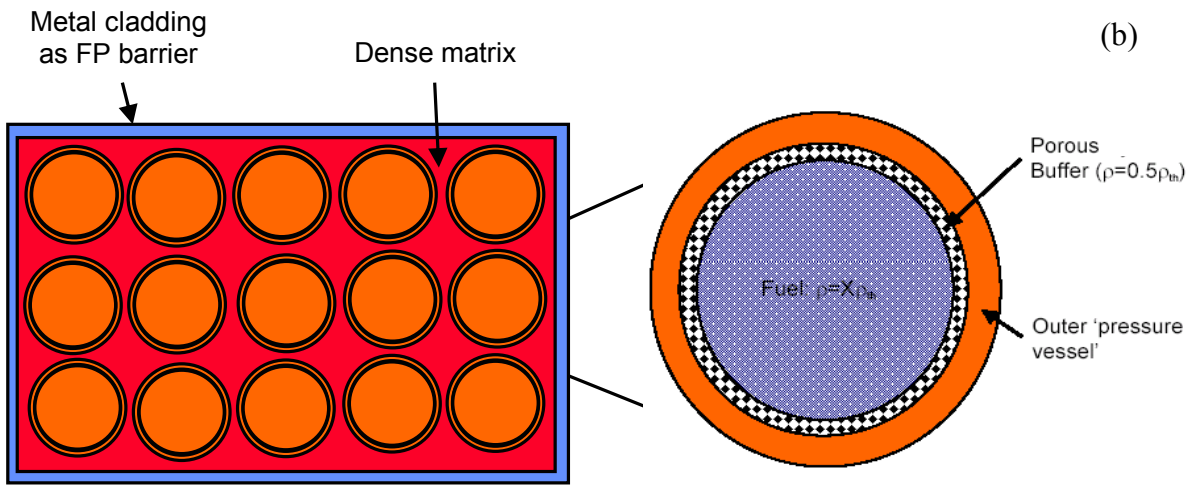
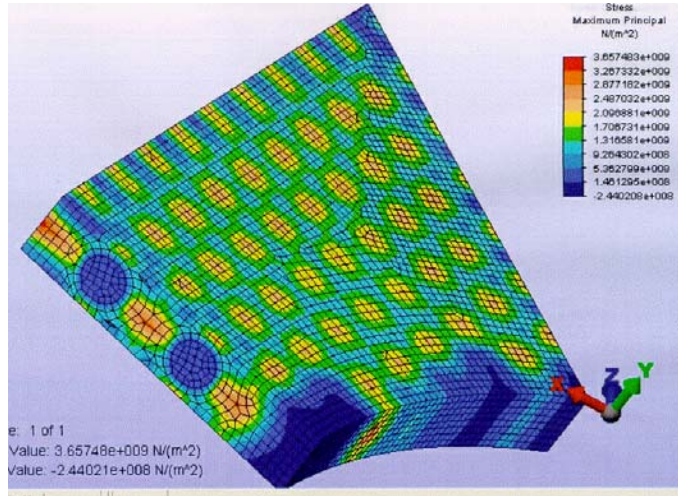


Figure 2.3. (a) FEA calculation of stress to the differential thermal expansion in a UC particle, SiC matrix dispersion. (b) 'Buffered' particle concept. (c) Plot of the effective stress in a coating due to fission gas pressure as a function of the shell thickness to kernel diameter ratio. Particle diameter 400 μm ; buffer thickness fixed at 19 μm .

There has been some recent development of TiN-based coatings for particle fuels [22]. ZrC has undergone irradiation testing as a coating on TRISO fuel, and may have superior retention of some fission products, especially at high-temperature. [23] There is, however, a much larger database available for fabrication, properties, and irradiation behavior of SiC coatings. [24]

Because of the existing SiC database, SiC coated (U,Pu)C kernels are selected as the reference materials for GFR dispersion fuels. The reference design includes a low density SiC buffer layer, preferably deposited from a non-halide source, and a dense SiC overcoat for fission gas retention.

2.4.3 Selection of Matrix Materials for Dispersion Fuel

A wide variety of initial choices for the matrix phase in a composite fuel are available including refractory metals, transition metals, oxide, carbide, and nitride ceramics as binary, ternary, and higher compounds, and intermetallic compounds. Recent related work on inert matrix fuels for plutonium and minor actinide burning has focused on determining the viability of cercer concepts using oxide matrices for plutonium burning in LWRs. This work has included fabrication studies [25,26], out-of-pile characterization, and irradiation testing of materials that employ uranium as a fissile surrogate for plutonium. [27, 28].

Requirements for GFR matrix materials are based on GFR performance requirements, Table 2.4 lists GFR fuel matrix material requirements based on reactor design goals as enumerated in Table 2.1.

Table 2.4. GFR fuel matrix material reference requirements

Requirement	Reference Value
Melting/decomposition temperature	>2000°C
Radiation induced swelling	< 2% over service life
Fracture toughness	> 12 MPa m ^{1/2}
Thermal conductivity	> 10 W/mK
Neutronic properties	Materials allow low core heavy metal inventory of less than 15 MT and maintain good safety parameters

Based on these requirements, the list of possible matrix material candidates is narrowed. Figure 2.4 (a) is a depiction of the periodic table. Elements that are gaseous or liquid at room temperature are shaded darkly, those with melting temperatures above ambient but less than 1800°C are noted with an intermediate shade of gray in a solid pattern. Elements with melting temperatures in the range of 1800° - 2000°C are shaded in light gray. Elements that meet the melting temperature criterion of 2000°C or above are left unshaded. (Tc is not considered here as a matrix material because it is radioactive, and there are limited quantities available in separated form for core startup). The transition

metals Ti, V, Cr, Fe, Ni and Zr, which are otherwise reasonable to consider as matrix materials, are thus excluded on the basis of inadequate melting temperature and lack of high-temperature creep resistance.

Figure 2.4 (b) considers additionally the impact of material neutronic properties on core heavy metal inventory and safety parameters. Scoping core neutronics studies [29] have shown that the use of the refractory metals Mo, Ta, W, and Re is not practical due to neutronic penalties associated with the high absorption cross sections of these materials that make it difficult or impossible to meet GFR design goals in terms of core heavy metal inventory and core safety parameters. Nb is marginal in this regard, and may be useable as a matrix material in some instances, when the volume can be limited. As discussed above, the combination of Nb cladding and ducts results in the requirement for large core heavy metal mass and degraded Doppler coefficient due to spectral hardening. Another potential option is the enrichment of naturally occurring molybdenum in the isotope ^{92}Mo , which dramatically decreases the absorption cross section. This is the approach being taken to the development of cermet Am targets as a part of the international FUTURIX-FTA irradiation program in the Phénix reactor. [30] This option has not been seriously pursued due to uncertainties in the cost of implementing molybdenum enrichment technology for large-scale deployment.

Carbon is also neutronically marginal due to the fact that it is a neutron moderator; limited quantities are possible in the core, however consideration of irradiation behavior eliminate carbon in the form of graphite or carbon-carbon composites. These materials exhibit anisotropic swelling under irradiation, resulting in severe degradation of mechanical properties at a dose of 10-15 dpa, far less than the estimated dose of ~ 160 dpa (stainless steel) expected for (non-fissile) fuel materials at the initial GFR goal burnup of 10 at.% HM. As seen in figure 2.4 (b), no materials in the elemental state are suitable for achieving GFR goals. This statement also applies in general to metal alloys. A possible exception is the use of niobium metal in small quantities. These considerations drive the choice of matrix materials into the realm of ceramics.

Ceramics, especially carbides and nitrides, tend to have high melting temperatures and excellent high-temperature creep resistance. There are thousands of possible binary, ternary, and higher ceramics based on combinations of elements with carbon, oxygen, nitrogen and sulfur; many of these materials have been poorly characterized with respect to properties. While intermetallic materials are a possibility, they also remain largely unknown in terms of general properties and irradiation behavior, and little can be said about the suitability of these materials for use in the GFR environment. Many of the refractory carbides and nitrides are again disqualified due to unsuitable neutronic properties. Table 2.5 (a) is a list of the more common and well characterized ceramics that meet screening requirements for melting temperature and core neutronics.

The criterion for thermal conductivity was established through the analysis of the stress generated by thermal gradients in a honeycomb matrix. The stresses in the honeycomb structure were found to be lower than those generated in a solid hexagonal block containing cylindrical coolant channels. Figure 5.4 (a) shows an example result of finite

element analysis of the temperature distribution in this body for a uniform power deposition of 70 MW/m^3 . Figure 5.4 (b) is a plot of the magnitude of the maximum temperature gradient in the body and the magnitude of the maximum principal stress calculated as a function of the bulk thermal conductivity of the matrix. It can be seen that at thermal conductivity values above about $12 \text{ W/m}\cdot\text{K}$, matrix stress is a slowly varying function of thermal conductivity. Below this value, matrix stress increases rapidly with decreasing thermal conductivity. The criterion for minimum thermal conductivity was thus set at $12 \text{ W/m}\cdot\text{K}$.

Considering the minimum thermal conductivity criterion leads to the elimination of most of the oxides and CeN, as shown in Table 2.5 (b). Further applying the criterion for irradiation stability of less than 2 volume percent of swelling during the in-core service life results in elimination of Si_3N_4 . Spinel (MgAl_2O_4) is marginal in this regard, and exhibits high swelling in response to high energy fission fragment damage, Mg in the spinel has been found to migrate down the temperature gradient during irradiation of spinel-matrix cermets, and so is disqualified. [31] While not strictly an irradiation performance issue, MgO has a high vapor pressure and poor thermal shock resistance, and is thus also disqualified. AlN also exhibits poor irradiation behavior in some temperature regimes (see below), and is considered marginal in this application. No data is available to support the selection of YC_2 , VC, or YN as matrix materials, so that they are not considered for use in the intermediate term.

After consideration of the screening criteria, a handful of materials emerge that have the potential to meet GFR fuel matrix material requirements. Based on available data, six ceramic materials and niobium have been selected for further study as potential matrix materials and coatings for GFR composite fuel concepts. The ceramics are zirconium carbide (ZrC), titanium carbide (TiC), silicon carbide (SiC), zirconium nitride (ZrN), aluminum nitride (AlN) and titanium nitride (TiN).

Despite common industrial use of many of these candidate matrix materials, there are still large gaps in mechanical and thermal property databases that make the design of a refractory ceramic matrix fuel form difficult. The response of many ceramic materials to neutrons and fission fragments is a complex function of cercer microstructure, irradiation temperature and dose history. Ceramics are also generally brittle and care must be taken that thermal and mechanical stresses in the matrix do not exceed the elastic limit of the material, or matrix cracking may occur, negating a fission product barrier and one of the useful attributes of this fuel. In addition, properties of ceramics are heavily dependent on the microstructure, and thus the route taken to fabrication. With this caution, material properties for the six ceramic materials are presented in Table 2.6. (Properties of niobium are discussed in section 2.4.3.7) In some cases there are large ranges or ambiguities in available data; these are indicated in the table.

The mechanical strength of ceramics is flaw controlled and thus depend strongly on specimen size and the number density and size of microstructural defects. Well characterized strength and fracture toughness data are not available for many of these materials due to the difficulty in processing the large number of specimens required to

obtain statistically significant data, and the lack of microstructural optimization. Many of these materials are used as coatings, so that bulk property data is not of great commercial interest. It can be expected that the strength and fracture toughness of specimens prepared by conventional powder processing will be similar to that of other materials in this class, ranging from 300-700 MPa when tested in four-point flexure. Fracture toughness and thermal shock resistance are issues that must be addressed for all ceramic materials through the use of microstructural designs that incorporate stable barriers to crack growth into the matrix. Each of the candidate matrix materials are discussed in the sections below.

H																	He		
Li	Be											B	C	N	O	F	Ne		
Na	Mg											Al	Si	P	S	Cl	Ar		
K	Ca	Sc	Ti	V	Cr	Mn	Fe	Co	Ni	Cu	Zn	Ga	Ge	As	Se	Br	Kr		
Rb	Sr	Y	Zr	Nb	Mo	Tc	Ru	Rh	Pd	Ag	Cd	In	Sn	Sb	Te	I	Xe		
Cs	Ba	La	Hf	Ta	W	Re	Os	Ir	Pt	Au	Hg	Tl	Pb	Bi	Po	At	Rn		
						Ce	Pr	Nd	Pm	Sm	Eu	Gd	Tb	Dy	Ho	Er	Tm	Yb	Lu

Figure 2.4 (a). Down-selection of matrix materials based on melting temperature criterion. Elements that are gaseous or liquid at room temperature are shaded darkly, those with melting temperatures above ambient but less than 1800°C are noted with an intermediate shade of gray in a solid pattern. Elements with melting temperatures in the range of 1800° - 2000°C are shaded in light gray. Elements that meet the melting temperature criterion of 2000°C or above are left unshaded.

H																	He		
Li	Be											B	C	N	O	F	Ne		
Na	Mg											Al	Si	P	S	Cl	Ar		
K	Ca	Sc	Ti	V	Cr	Mn	Fe	Co	Ni	Cu	Zn	Ga	Ge	As	Se	Br	Kr		
Rb	Sr	Y	Zr	Nb	Mo	Tc	Ru	Rh	Pd	Ag	Cd	In	Sn	Sb	Te	I	Xe		
Cs	Ba	La	Hf	Ta	W	Re	Os	Ir	Pt	Au	Hg	Tl	Pb	Bi	Po	At	Rn		
						Ce	Pr	Nd	Pm	Sm	Eu	Gd	Tb	Dy	Ho	Er	Tm	Yb	Lu

Figure 2.4 (b). Down selection of matrix materials based on neutronic and irradiation behavior criteria. Materials that meet other criteria but are neutronicly unacceptable are shaded with a horizontal grid; materials are excluded on the basis of irradiation behavior are shown with a diagonal grid. No elemental materials meet GFR requirements, although Nb is marginal.

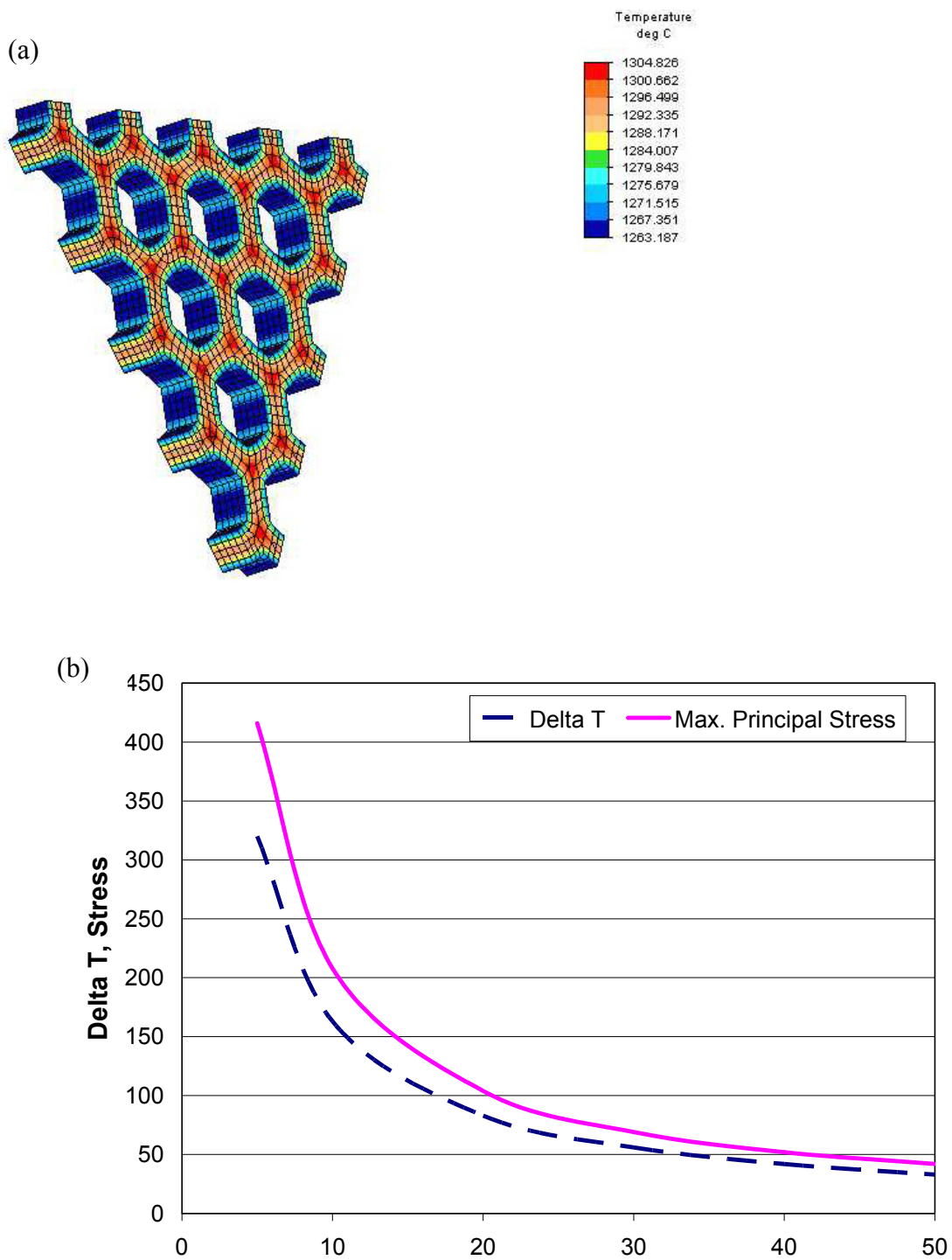


Figure 2.5. Effect of thermal conductivity on thermal gradients and matrix stress for a power density of 140 MW/m^3 . (a) Example of results of FEA calculation for temperature distribution. (b) Plot of magnitudes of maximum temperature gradient and maximum principal stress over matrix thermal conductivity in W/m-K .

Table 2.5 (a) Ceramics that meet melting temperature and neutronics requirements.

Oxides	Carbides	Nitrides
Al ₂ O ₃	SiC	AlN
CeO ₂	TiC	CeN
MgAl ₂ O ₄	VC	Si ₃ N ₄
MgO	YC ₂	TiN
Y ₂ O ₃	ZrC	YN
ZrO ₂		ZrN

Table 2.5 (b) Ceramics that meet melting temperature, neutronics, and thermal conductivity requirements.

Oxides	Carbides	Nitrides
Al ₂ O ₃	SiC	AlN
CeO ₂	TiC	CeN
MgAl ₂ O ₄	VC	Si ₃ N ₄
MgO	YC ₂	TiN
Y ₂ O ₃	ZrC	YN
ZrO ₂		ZrN

Table 2.5 (c) Ceramics that meet melting temperature, neutronic, and irradiation performance requirements.

Oxides	Carbides	Nitrides
Al ₂ O ₃	SiC	AlN
CeO ₂	TiC	CeN
MgAl ₂ O ₄	VC	Si ₃ N ₄
MgO	YC ₂	TiN
Y ₂ O ₃	ZrC	YN
ZrO ₂		ZrN

Table 2.6. Summary of properties of candidate GFR matrix materials.

Property	SiC	ZrC	TiC	AlN	TiN	ZrN
Theoretical Density (g/cm ³)	3.21 (β)	6.51	4.91	3.25	5.42	7.35
Fracture Toughness (MPa m ^{0.5})	4-6	--	--	3-4	5	4-7
Elastic Modulus (GPa)	480	400	450	350	250-590	380-510
Shear Modulus (GPa)	162	--	--	--	--	154
Poisson's Ratio	0.17	0.19	--	0.22	0.22	0.26
Flexural Strength @RT (MPa)	700	--	400	300-500	430	--
Compressive Strength @RT (GPa)	4.6	--	0.7-3.0	--	1.3	1.0
Specific Heat Capacity (Range 20-1000°C)(J/kg.K)	700-1300	250-500	550-880	800-1000	800-1000	800-1000
Melting Temperature (°C)	2760	3450	3067	2790 (decomp)	2950	2980
Thermal Conductivity (W/m.K)	40-120	17-36	10-20	100-200	20-60	10-15
Thermal Expansion Coeff. (10 ⁻⁶ /°C) (RT-1000°C)	5.3	6.7	8.3	5.0	9.4	7.2

2.4.3.1 SiC

SiC offer the largest existing database in terms of material properties, irradiation behavior, and fabrication. Silicon carbide exists in cubic, hexagonal and rhombohedral structures. The hexagonal and rhombohedral structures are referred to as α -phase, while the cubic phase is referred to as the β -phase. SiC rapidly forms an SiO₂ surface scale on exposure to air at elevated temperature. This surface layer is compact and offers protection from further oxidation. SiC thus has excellent oxidation resistance, for example SiC heating elements have a service life of thousands of hours at surface temperatures exceeding 1600°C. The irradiation behavior of SiC is well documented. The understanding of the irradiation behavior of SiC-based composite materials is also maturing [32], and can be applied should the use of a composite be required to increase fracture toughness. Processing of SiC into dense shapes is currently done on an industrial scale at a reasonable cost, although major modifications will be required for processing of particle fueled composites. Other properties of SiC appear to be adequate for GFR service, with the exception of low fracture toughness. SiC is thus selected as the reference matrix material for initial GFR fuel development.

With the exception of SiC, irradiation behavior data for the other carbide and nitride ceramics considered is sparse, although the data that does exist indicates mostly benign response to irradiation. These alternate materials may however, offer benefits due to their more refractory nature and additional opportunities for fabrication processes and property tailoring to meet specific GFR fuel needs.

2.4.3.2 ZrC

Zirconium carbide is an extremely refractory material, but also very difficult to process due to low intrinsic diffusion coefficients even at temperatures in excess of 2000°C. ZrC forms in the face-centered cubic ‘rock-salt’ structure (sodium chloride prototype, as do TiN, ZrN, and TiC). [33] ZrC is the sole compound that forms in the Zr-C system, and has a wide solubility range, from 37.5 to 49.4 atom % carbon (7.3 -11.4 wt.%) at 1835°C. The highest melting point is achieved at a composition of 44.5 at.% carbon (9.5 wt.%). The minimum solidus temperature of the two-phase mixture that forms for carbon rich material is 2910°C. This is of interest due to the possibility of increasing fracture toughness through the presence of graphite platelets in the microstructure. The solidus temperature of hypostoichiometric compositions is ~1835°C; this may also be acceptable as it is likely that a material containing a small fraction of free zirconium metal will maintain adequate structural integrity during a GFR loss of coolant condition. Barnier et. al. [34] studied the hot-pressing kinetics of ZrC in the temperature range from 1700°-2400°C and a pressure of 40 MPa. Data were collected for processing times of one and two hours. Theoretical density of greater than 95% was achieved at 1900°C after two hours or at 2000°C for one hour. Thermal conductivity in ceramics can vary widely with microstructure and impurity content. At 1000°C, data for ZrC indicates that thermal conductivity values range from approximately 17 to 36 W/mK. [35,36,37] Limited data on the neutron irradiation behavior of ZrC is available. Specimens of slip cast/sintered and explosion pressed ZrC were irradiated in the ETR (Engineering Test Reactor) in the late 1960’s at two different temperatures (130-355°C and 1000°-1100°C) to a fast neutron fluence of 5×10^{21} n/cm². [38] Volume swelling in the lower temperature range was on the order of 3%. As is common in ceramics, irradiation at higher temperatures results in less swelling due to self-annealing (recombination) of neutron produced defects. Swelling was 1% or less at the higher irradiation temperature. ZrC has been used as a coating in TRISO-type fuel. [39,40] In this capacity, it seems to have performed well under irradiation when deposited as a CVD coating. No quantitative data on swelling or changes in other physical attributes is available from these tests, however.

2.4.3.3 TiC

Similar to ZrC, the TiC phase has a wide stoichiometry range on the hypostoichiometric side of the 1:1 compound phase. Properties such as hardness and melting point vary with stoichiometry with the highest melting point being at the TiC_{0.44} composition. The maximum melting temperature is ~3070°C, with a minimum solidus temperature of ~2780°C for the carbon-rich eutectic. Kendall [41] reported extensive work on arc casting of hyperstoichiometric TiC using a water-cooled graphite hearth. Work was focused on producing specimens containing free carbon to improve thermal shock

resistance. The strength of these materials produced by arc casting were measured in flexure and compression, and indicate that behavior and strength is typical of other ceramics in this class. Because of its high melting point and low atomic number, TiC is a candidate material for in-vessel component coating material for fusion devices. As such, irradiation property studies have focused on high-energy helium ion bombardment effects. [42,43] Limited data on the neutron irradiation behavior of TiC is available. Specimens of slip cast and sintered and explosion pressed TiC were irradiated in in the same test as discussed above for ZrC. Behavior under those conditions is similar to that of ZrC, with swelling of material irradiated at low temperatures in the range of 2-3 vol.%, and swelling of material irradiated at the higher temperature in the range of 0.25-0.5 vol.%.

2.4.3.4 AlN

Refractory nitride compounds offer another opportunity for matrix material optimization. The use of natural nitrogen in these compounds, however, leads to the production of ^{14}C , which is a concern from both the perspective of release during recycle and core neutron economy. The repercussions of nitrogen enrichment and recovery on fuel cycle costs are not fully understood, and the acceptability of nitrides as fuel and matrix materials in the GFR core thus remains an open question. Despite this question, nitride compounds may have advantages over carbides in terms of processability, thermal conductivity, and irradiation stability, and so are considered as GFR matrix materials.

Aluminum nitride (AlN) is used widely in the electronic industry in heat sink and heat exchanger applications, semi-conductor multi-layer substrates, and crucibles. AlN has a Wurtzite type hexagonal close packed (HCP) crystal structure; aluminum atoms are arranged in the HCP structure with nitrogen atoms filling one half of the tetrahedral sites [44]. AlN has a very narrow stoichiometry range and melts incongruently. The decomposition temperature under one atmosphere of nitrogen is 2417°C . Fabrication of components with density in excess of 99% is achieved routinely on a commercial scale. Typical densification processes used for fabricating AlN include tape casting, slip casting, or dry pressing followed by pressureless sintering or hot pressing. Because of the strong covalent nature of bonding, high temperatures (1800°C) are needed for sintering. Oxides of lanthanide, yttrium, or alkaline earth metals are commonly used as sintering aids. Thermal conductivity has been theoretically calculated to be as high as $320\text{ W m}^{-1}\text{ K}^{-1}$ and measured as high as $285\text{ W m}^{-1}\text{ K}^{-1}$ in high purity materials. [45] More typical values are $36\text{ W/m}\cdot\text{K}$ at 1000°C . [46] The coefficient of thermal expansion at lower temperatures is $4.4\times 10^{-6}\text{ K}^{-1}$. This is a relatively low value, which when coupled with good thermal conductivity, provides for better shock resistance than most ceramics [47]. Aluminum nitride neutron irradiation properties have been studied at both high and low fluence in a fast neutron spectrum. It was found that AlN exhibited strong anisotropic swelling above $2.4\times 10^{24}\text{ n/m}^2$ (470°C) as would be expected by the HCP structure, however it was reported that swelling was isotropic at a fluence of $8.3\times 10^{22}\text{ n/m}^2$ (100°C). Overall swelling was reported to be less than that found for silicon carbide at similar fluences. Specimens increased 0.15% in volume when irradiated to $5.3\times 10^{25}\text{ n/m}^2$. Upon microstructural investigation no cracks or voids were visible. In the

fluence range of 8×10^{24} – 2×10^{25} n/m² microcrack formation on the grain boundaries was noted due to anisotropic swelling. [48,49] Relatively high bending strengths (>350 MPa) were maintained on irradiation to 5.3×10^{25} n/m². At a fluence of 9.1×10^{25} n/m², however, bending strength was reduced to less than 10 MPa due to the microcracking discussed above. Thermal diffusivity decreased nearly 20% on specimens irradiated to 8.3×10^{22} n/m². Thermal diffusivity decrease with further irradiation was minimal.

2.4.3.5 TiN

Titanium nitride (TiN) is used extensively as a hard coating on machine cutting tools. This material is applied using various well-developed coating methods. The properties and mechanical properties of monolithic solids are not well studied, however. TiN has a wide range of nitrogen solubility, although the nitrogen rich portion of the phase diagram is not well documented. Thermal conductivity data is sparse. As is typical for materials in this class, indications are that thermal conductivity varies strongly with microstructure. Values likely range from 15-25 W/m·K. [50] A TiN specimen irradiated in the Phénix reactor showed no detectable swelling on radiographic examination after a fast neutron fluence ($E > 0.1$ MeV) of $1.95 \cdot 10^{26}$ m⁻². [51]

2.4.3.6 ZrN

Similar to TiN, ZrN is used primarily as a coating material for machine tools such as drill bits, rotary files, and milling cutters. Also like TiN, ZrN has a face-centered cubic rock salt (NaCl) crystal structure. Little reliable data is available on properties of monolithic materials of interest to fuel developers. [52] ZrN has a wide solubility range, however the nitrogen rich side of the phase diagram is not well known. ZrN has a melting temperature of $\sim 2980^\circ\text{C}$, second only to HfN in the nitride class. Irradiation testing of ZrN as a non-fertile matrix for destruction of plutonium and minor actinides is planned or has been executed in several countries. Solid solution pellets of (Pu,Zr)N and two phased TiN + PuN pellets have been fabricated and are undergoing irradiation testing. [53] Fuel fabrication activities focused on (Pu,Zr)N are also conducted in Switzerland as part of the CONFIRM program [54] and in the U.S. as part of the AFC (Advanced Fuel Cycle) program. No irradiation performance data is yet available for these fuels. Irradiation with 450 keV Xe³⁺ ions and 13 keV He⁺ ions is currently underway at Los Alamos National Laboratory, however final results on swelling behavior are not yet available.

2.4.3.7 Niobium Alloys

Niobium alloys are relatively well known in terms of properties and irradiation behavior, Nb-1Zr having been extensively developed as a cladding material during the SP-100 space reactor program and subject to irradiation dose exceeding that required to achieve the initial GFR goal burnup. [55] Detailed data on the properties of Nb alloys in general including oxidation resistance, temperature and strain rate dependent mechanical properties, properties as a function of impurity content, and fabrication can be found in [56]. A more recent tabulation and assessment of properties and correlations is found in

[57]. Some detailed information on irradiation behavior is available [58]; Figure 2.6 is a plot of irradiation induced swelling as a function of temperature based on data circa. 1984, that shows a peak swelling temperature of about 800°C. Because of its demonstrated good irradiation performance as both a matrix material in cermet fuels (discussed below) and as a cladding material, niobium is retained as a backup candidate as both cladding and matrix material.

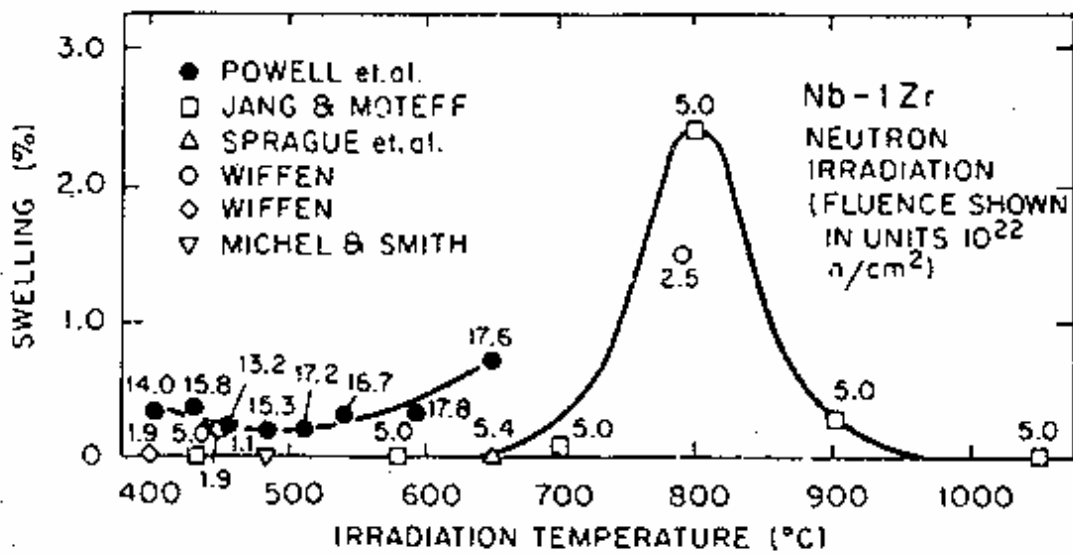


Figure 2.6. Irradiation behavior of Nb-1Zr as a function of temperature.

2.4.4 Reference and Alternate Dispersion Fuel Concepts

2.4.4.1 Reference Dispersion Fuel Concept

Because of the acceptable properties of SiC, the large irradiation behavior database, the preference of core designers for SiC over Nb, and the experience in use of SiC as a component in TRISO fuel, a dispersion of (U,Pu)C particles coated with a bi-layer SiC coating in a SiC matrix is selected as the reference GFR fuel concept. This selection is made with the realization fuel density is marginal, improvements in fracture toughness are required, as is the potential use of an outer cladding on block-type elements. Reference fuel parameters are listed in Table 2.7.

Table 2.7. Reference GFR dispersion fuel parameters

Parameter	Reference Value
Fuel particle type	Bi-layer SiC coated (U,Pu)C, Two size distribution (1) 1.64mm diameter (2) 480 μm diameter
Inner coating	Buffer layer of SiC with TD<30% and low crush strength (1) buffer thickness $\sim 58 \mu\text{m}$ (2) buffer thickness $\sim 17 \mu\text{m}$
Outer coating	Dense CVD SiC, (1) thickness $\sim 61 \mu\text{m}$ (2) thickness $\sim 18 \mu\text{m}$
Fuel kernel	(U,Pu)C (1) 1.4 mm diameter (2) 410 μm diameter
Heavy metal density	6 g HM $\cdot\text{cm}^{-3}$, 75% particle loading 5 g HM $\cdot\text{cm}^{-3}$, 63% particle loading
Matrix	Dense SiC

Outer coating thicknesses have been specified to protect the buffer layer during handling of the coated particles. In order to increase particle packing density, a dual sized distribution of particles is specified.

Fabrication of this fuel type will be difficult due to the high particle loading and the fragile nature of the coated particles, and will require novel processing techniques. The reference fabrication process is infiltration and reaction bonding, as sintering will not be effective and hot pressing will likely damage the thinly coated particles. CVD processing is not likely to be effective in filling the channels within the packed bed.

In order to fabricate the composite fuel, particles may be precoated with a carbonaceous precursor and then assembled into a packed bed or assembled into a packed bed and then infiltrated with a carbonaceous precursor [59]. The precursor is then thermally converted to carbon. After conversion, the matrix is infiltrated with molten silicon, and thermally treated to allow reaction of the silicon with carbon. Many variations on this method may

be possible, including substitution of a portion of the SiC outer shell with pyrocarbon in order to encourage bonding of the matrix to the fuel particles, or treating the particles to discourage bonding to the matrix.

The fact that the infiltration technique has been used previously to fabricate fuel that was successfully irradiation tested lends some credibility to the process. Figure 2.7 shows lateral and transverse cross-sectional images of a fuel rod (1.27 cm diameter) consisting of a dispersion of pyrocarbon coated particles in a SiC matrix formed by reaction bonding. [60] This fuel was fabricated and irradiation tested as part of the high temperature AGR (Advanced Gas Reactor) fuel development effort in Great Britain. Irradiation experiments were conducted at temperatures between 750 and 1200°C and rod powers of 39 kW/m in two experiments. Burnup values ranged from 1.6 to 5% FIMA. Fractional fission gas release was measured during low burnup tests, and was found to be on the order of 10^{-6} .

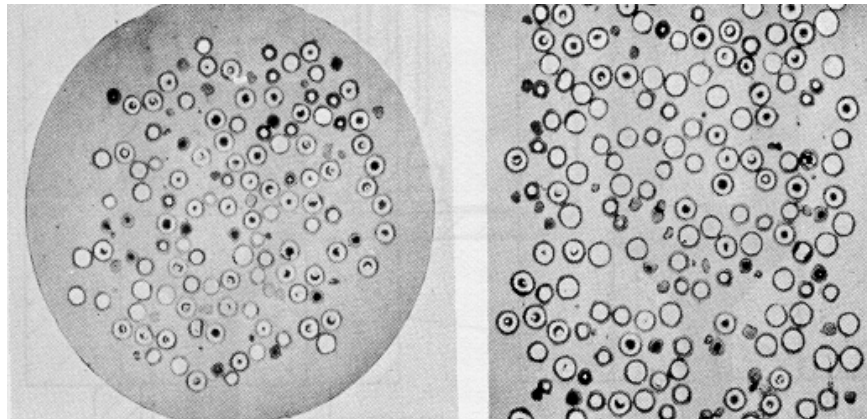


Figure 2.7. SiC matrix coated particle fuel fabricated by reaction bonding.

2.4.4.2 Alternate Dispersion Fuel Concept

Due to the novel nature and uncertainties in irradiation performance of the reference SiC matrix GFR fuel, an alternate dispersion fuel based on a niobium matrix is proposed. This fuel has also been irradiation tested to burnups and temperatures consistent with GFR reference design goals, and at much higher heavy metal densities than SiC matrix fuel. Figure 2.8 shows a postirradiation image of a dispersion of UO_2 particles in a niobium matrix. [61] The fuel loading in this case is 80 percent by volume. The fuel was fabricated by first CVD coating fuel particles with niobium, then isostatically pressing at 1260°C at 10,000 psi (69 MPa) for 3 hours. The fuel was subject to irradiation at a fuel centerline temperature of 1480°C to approximately 4 at.% burnup. After irradiation, the fuel exhibited a density decrease of 1.4%. Fuel heavy metal density in this case is on the order of 6.7 g/cm^3 . It is recommended that this fuel be reevaluated in terms of GFR system neutronic and safety performance.

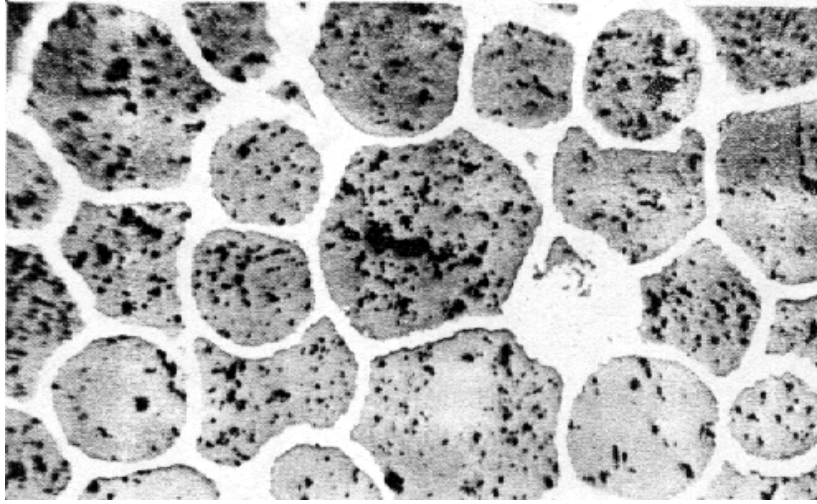


Figure 2.8. Postirradiation metallograph of an 80 vol.% dispersion of UO_2 in Nb irradiated at $T > 1400^\circ\text{C}$ to $\sim 4\%$ burnup.

3.0 EFFECT OF MINOR ACTINIDES ON FUEL PERFORMANCE

Neutron capture by ^{241}Am and subsequent decay of the ^{242}Cm capture product leads to production of helium gas as in Figure 3.1. This helium generation adds to the total gas inventory, which can become significantly higher than the gas inventory due to fission. The generation of helium gas during transmutation of ^{241}Am is thus a significant issue that must be accounted for in the design of fuels that contain significant quantities of minor actinides.

Other changes in fuel the behavior of MA-bearing fuel relative to conventional U-Pu fuels are due to changes in fission product element distribution which affect the chemical interaction behavior of the fuel with surrounding materials. Thermal conductivity is also a potential issue; the thermal conductivity of Am-bearing compounds has been found to be lower than U,Pu analogs. The impact of these effects on fuel behavior is more difficult to gauge.

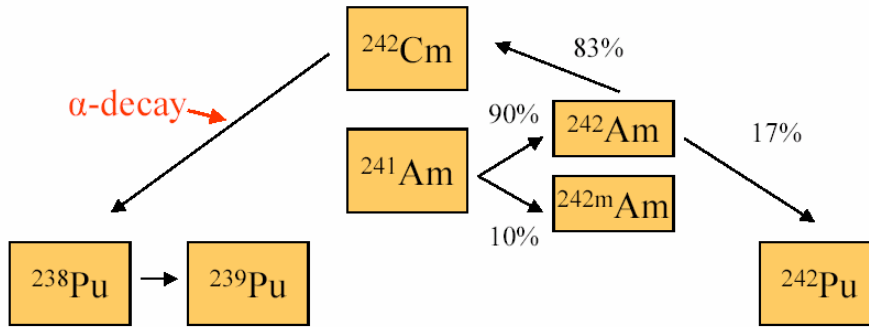


Figure 3.1. Capture and decay chain for ^{241}Am resulting in He gas generation.

Of all of the potential impacts of MAs on fuel behavior, helium generation is likely to be the largest; the minor actinide isotope of primary concern from a fuel performance perspective is therefore ^{241}Am . Other MAs increase fuel gas inventory by a lesser amount.

3.1 Experimental Data for Helium gas generation

There are four known experiments involving transmutation of ^{241}Am . Results from two, the EFTTRA-T4 test and the SUPERFACT-1 experiment have been published. Comprehensive results from two additional experiments, the ANL X501 experiment and a BNFL oxide experiment have not been published. Some data on helium generation is available for each experiment, and the results are analyzed here and presented in a uniform set of units for comparison. The quality and completeness of data vary for each experiment; therefore the results of this analysis contain a good deal of uncertainty, and do not provide a good basis for extrapolation.

3.1.1 EBR-II X501 Experiment

The X501 experiment was conducted in EBR-II to demonstrate minor actinide burning through the use of a homogeneous recycle scheme. The X501 subassembly contained two metallic fuel elements loaded with relatively small quantities of americium and neptunium. The attributes of these elements are given in Table 3.1. X501 was inserted into EBR-II for run 163, beginning on February 1993, and withdrawn just prior to shutdown in August 1994. Total irradiation time was approximately 339 EFPD's. Burnup, calculated on the basis of REBUS/RCT/ORIGEN data was 7.6% HM with transmutation of 9.1% of ²⁴¹Am. Plenum helium volume was measured by gas sampling, and agrees reasonably well with the calculated data. Since the fill gas was Ar-25He, and the fill volume is not known, the assumption was made that all argon fill gas was recovered on postirradiation gas sampling. The initial helium fill gas volume was then calculated by using the Ar:He ratio. Data relevant to the calculation of specific helium gas generation are given in Table 3.2. The helium generation rate is presented in units of cubic centimeters of helium at STP (standard temperature and pressure) per gram of ²⁴¹Am transmuted, for comparison with other data. Helium generation rate is calculated to be in the range of 38.6-44.8 cm³ He per gram of americium transmuted, depending on the value used for postirradiation helium inventory.

Table 3.1. Attributes of X501 minor actinide bearing fuel elements.

Composition (average wt%)	U-20.2Pu-9.1Zr-1.2Am-1.3Np
Major impurities (average wt%)	Si:0.26, Al:0.089, Ca:0.067, Cr:0.0025, Mg:0.009, Fe:0.001, Mn:0.001
U-235 enrichment (nominal)	60%
Fuel mass	77.5 g
Fuel length	34.3 cm (13.5 in.)
Element length (nominal)	74.9 cm (29.5 in.)
Cladding OD	5.84 mm (0.230 in.)
Cladding wall	0.457 mm (0.018 in.)
Slug diameter	4.27 mm (0.168 in.)
Plenum volume	7.1 cm ³
Plenum gas	Ar-25He
Smear density	75%
Fuel slug density, % theoretical	99.5%
Estimated peak linear heat generation rate	45 kW/m (13.7 kW/ft)
Estimated fuel peak centerline temperature	700°C
Estimated cladding inner surface temperature	540°C

Table 3.2. Parameters used in calculating He gas generation rate for X501 pin G582.

Parameter	Value	Data source
BOL ²⁴¹ Am content	0.972 g	ANL chemical analysis samples 92-2087-01 to -06
EOL ²⁴¹ Am content	0.884 g	McKnight REBUS/RCT/ORIGEN analysis
²⁴¹ Am transmutation	0.088 g (9.1 %)	
Measured He in plenum	3.94 cm ³	Based on AGHCF gas sampling (sample 505A1A, 12/15/95) with assumptions about He volume in initial fill gas
Calculated He inventory	3.4 cm ³	McKnight REBUS/RCT/ORIGEN analysis decayed to 6/01/96
Specific He gas generation	38.6-44.8 cm ³ /g	He gas volume at STP per gram of ²⁴¹ Am transmuted

3.1.2 SUPERFACT-1 Experiment

SUPERFACT-1 was irradiated in the Phénix reactor from October 1986 to January 1988. Attributes of the high americium SUPERFACT-1 pins are given in Table 3.3. In addition to two high americium elements, (U-45Np)O₂, (U-24Pu-1.8Am)O₂, and (U-24Pu-1.5Np)O₂ were also irradiated. Gas inventories were measured by vacuum evaporation, and are given in Table 3.4. The He:FG ratio of 4.7 is somewhat lower than the value of 6.0 calculated for the thermal spectrum EFTTRA-T4 test.

Table 3.3. Attributes of SUPERFACT-1 americium-bearing fuel elements.

Composition	(DU-19.2Am-21.2Np)O ₂
Fuel column length	39.9 cm (15.7 in.)
Element length (nominal)	179.3 cm (70.6 in.)
Cladding OD	6.55 mm (0.258 in.)
Cladding wall	0.45 mm (0.018 in.)
O/M ratio	1.927
Plenum volume	7.1 cm ³
Plenum gas	He
Smear density	89%
Estimated peak linear heat generation rate	17.4 –27.3 kW/m (13.7 kW/ft)

Table 3.4. Gas sampling data for SUPERFACT-1.

Composition (wt%) (nominally MO ₂)	%HM burnup	Kr + Xe (cm ³)	He (cm ³)	He:FG
(U-28Pu)O ₂	8.5	235	10.3	0.04
(U-24Pu-1.8Am)O ₂	6.8	153	39.9	0.26
(U-45Np)O ₂	4.6	141	22.9	0.16
(U-19.2Am-21.2Np)O ₂	4.3	134	631	4.7
(U-24Pu-1.5Np)O ₂	6.8	153	14.4	0.09

Data comparisons of SUPERFACT to the EFTTRA-T4 report (EUR 19138 EN) was used to estimate specific helium release; these data are shown in Table 3.5. These numbers are calculated for EOI (end-of-irradiation) and after one year cooling. The helium gas inventory increases with cooling time due to decay of ²⁴²Cm, which has a 163 day half-life. This causes the specific helium gas generation rate to increase from 33.3 cm³/g ²⁴¹Am transmuted at EOI to 63.4 cm³/g ²⁴¹Am after cooling. The latter number should be compared to the specific generation rate of 38.6-44.8 cm³/g for X501.

Table 3.5. Parameters used in calculating He gas generation rate for SUPERFACT-1 Am-bearing pins.

Parameter	Value	Data source
Calculated He inventory, EOI	7.12x10 ⁻⁴ mol He/cm ³ fuel (16.0 cm ³ He/cm ³ fuel)	Table 7.1 of Euratom report
Calculated He inventory, 1 year cooling	1.36x10 ⁻³ mol He/cm ³ fuel (30.5 cm ³ He/cm ³ fuel)	EUR 19138 EN compares SUPERFACT-1 to EFTTRA-T4
BOL ²⁴¹ Am content	1.89 g Am/cm ³ fuel	Calculations based on information in Walker, JNM 218 (1995) 129-138 and Prunier, Proc. FR'91 Vol. II.
²⁴¹ Am transmutation	0.481 g Am/cm ³ fuel (25.4 %)	
Specific He gas generation at EOI	33.3 cm ³ /g	He gas volume at STP per gram of ²⁴¹ Am transmuted
Specific He gas generation at 1 year cooling	63.4 cm ³ /g	

3.1.3 Thermal Spectrum EFTTRA-T4 Experiment

The EFTTRA-T4 experiment [62] was irradiated in hafnium filtered thermal flux at the High Flux Reactor (HFR, Petten, The Netherlands). The EFTTRA-T4 experiment consisted of ²⁴¹Am bearing oxide particles incorporated in an inert oxide matrix (MgO·Al₂O₃ spinel). Test parameters and some test results from EFTTRA-T4 are given in Table 3.6.

Table 3.6. Parameters and some results of the EFFTRA-T4 ²⁴¹Am transmutation test.

Temperature (aluminum carrier near cladding)	400°-450°C
Fuel phases (some uncertainty)	MgO·Al ₂ O ₃ spinel + ~3 μm dia. (Am,Al)O ₃ (?) particles
²⁴¹ Am loading	9.7-11.9 wt%
Duration of irradiation	358.4 EFPD's
²⁴¹ Am transmutation	96%
Total actinide burnup	28%
Total fluence (calculated)	3.5 x 10 ²⁶ m ⁻²
Fluence > 0.1 MeV (calculated)	1.7 x 10 ²⁶ m ⁻²
Volumetric pellet swelling	~18%

Generation of helium during irradiation caused high fuel swelling and significant fuel cladding mechanical interaction. The helium release rate from the fuel was much higher than the fission gas release rate. Gas pressure after one year of cooling was 0.5 MPa, of which 94.9 vol% was helium. As seen in Table 3.7, the inventory of helium was nearly sixfold that of fission gas, and the volume release of helium from the fuel was twenty-two times that of fission gas.

Table 3.7. Gas inventories and release at end of life in EFFTRA-T4 (one pin).

Gas species	Inventory, moles	Release, moles	%Release
He	1.37E-03	2.66E-04	22.3
Kr	8.92E-06	1.07E-06	11.9 ^a
Xe	2.20E-04	1.08E-05	4.9
He:fission gas ratio	5.98	22.3	-

a) The authors of EUR 19138 EN consider this value suspect, since the measured quantity of Kr was near the detection limits of the apparatus.

Parameters used to calculate the helium gas generation rate are given in Table 3.8. No experimental verification of calculated helium inventory was conducted. Helium generation rate was calculated to be 44.8 cm³ per gram of americium transmuted at end-of-irradiation and 59.9 8 cm³ per gram of americium transmuted after one year cooling.

Table 3.8. Parameters used in calculating He gas generation rate for EFTTRA-T4.

Parameter	Value	Data source
Calculated He inventory, EOI	1.37×10^{-3} mol He (30.7 cm ³)	Table 6.2 of Euratom report EUR 19138 EN, MCNP-FISPACT calculations at EOI (end-of-irradiation) and after 1 year cooling.
Calculated He inventory, 1 year cooling	1.73×10^{-3} mol He (38.7 cm ³)	
BOL ²⁴¹ Am content	0.685 g	
²⁴¹ Am transmutation	0.646 g (94.9 %)	
Specific He gas generation at EOI	44.8 cm ³ /g	He gas volume at STP per gram of ²⁴¹ Am transmuted
Specific He gas generation at 1 year cooling	59.9 cm ³ /g	He gas volume at STP per gram of ²⁴¹ Am transmuted

3.1.4 PFR Sesquioxide Experiment

Three types of oxide fuel pellets were fabricated at Oak Ridge National Laboratory (ORNL-TM-5858) and assembled into small fuel pinlets at Hanford (HEDL-7057). The pinlets were shipped to Dounreay for assembly into an irradiation test vehicle and for insertion in the PFR (Prototype Fast Reactor) by BNFL. Information on this experiment has not been published in the open literature. Pellet, fuel pinlet, and irradiation parameters are given in Table 3.9. After one cycle of 63 EFPDs, the experiment was withdrawn from the reactor for an interim examination at approximately 1.6% HM burnup. Gamma radiography showed that the fuel column in the Cm₂O₃ sample had grown approximately 80% in length. The experiment was not reinserted in the reactor, and further examination commenced on all MA-bearing fuel samples. The FISPIN code was used to calculate gas production; data are summarized in Table 3.10. The calculated value of 68.8 cm³ He per gram transmuted americium (EOI) appears high relative to other data presented here. This is likely due to uncertainty in calculation of the small amount of americium transmutation.

Table 3.9. Fuel Parameters for joint DOE/UKAEA Actinide Burning Test

Fuel Compositions	Am ₂ O ₃ , Cm ₂ O ₃ , (Am ₆ La ₇ Cm) ₂ O ₃ La:Ce:Nd:Sm
Isotopes	²⁴¹ Am, ²⁴⁴ Cm
Pellet Diameter	0.150" (3.8 mm)
Smeared Density	80-86%
Cladding	D9, 0.230" OD, 0.030" wall (5.83/0.76 mm)
Fuel Column Length (approx.)	1.5-2" (40-50 mm)
Plenum:Fuel Length Ratio (approx.)	~1:1
Linear Power	9-10.5 kW/m
Irradiation Time	63.4 EFPD's
Burnup	~1.6 at% (initial HM inventory?)
Peak Temperature	T _{CL} < 800°C

Table 3.10. Data relevant to calculation of specific He gas generation for Am₂O₃ pin

Parameter	Value
Calculated He inventory	1 cm ³ /g
BOL ²⁴¹ Am content	0.909 g/g fuel
²⁴¹ Am transmutation	0.015 g (1.6 %)
Specific He gas generation (EOI)	68.8 cm ³ /g

3.1.5 Implications of ²⁴¹Am loading GFR fuel design

A summary of the estimates for specific helium gas generation are given in Table 3.11. Values range from 33.3 to 68.8 cm³ He/gram of ²⁴¹Am transmuted. Variations may be due to differences in data quality, core neutron spectra, the arrangement of irradiation and cooling cycles, uncertainties in cross sections for ²⁴²Cm formation, and the method used for estimating helium generation. The data in Table 3.11 do not lend themselves well to extrapolation, but provide an indication of the volumes of gas that must be taken into account during fuel design. When comparison of the ratios of helium to fission gas is made, it can be seen that a rough rule of thumb is that at 20% loading of ²⁴¹Am by mass results in a doubling of the fuel gas inventory. The helium gas produced is also much more mobile than xenon and krypton, and thus much more likely to be released from the fuel microstructure into the plenum region of pin-type fuels or the buffer region of particle fuels. The higher gas inventory and higher He gas release rate results in increase stress on cladding, particle coatings, and dispersion fuel matrices. The impact of helium production on fuel design thus becomes significant for pins containing more than 10 wt% ²⁴¹Am, and becomes overwhelming for fuel with high americium content.

Table 3.11. Summary of experimental helium gas generation data for Am-bearing fuels

Test	Specific He generation (cm ³ He at STP/gram of ²⁴¹ Am transmuted)	Notes
X501	38.6-44.8	14-21 months cooling
SUPERFACT-1	33.3-63.4	EOI - 1 year cooling
EFTTRA-T4	44.8-59.9	EOI - 1 year cooling
PFR 0402AE	68.8	EOI

3.2 Other factors

Other factors that are likely to be factors in the determination of fuel behavior and fuel lifetime limits are the change in the fission product chemistry of TRU loaded systems and potentially decreased thermal conductivity at high TRU loadings.

Changes in fission product distribution that result from fission of the heavier actinides. These differences may result in differences in fuel/cladding chemical interaction (or fuel/matrix chemical interaction) behavior. Also possible are changes in nitrogen partial pressure for nitride fuels as a result of an increase or decrease in nitrogen scavenging fission products. Analysis of these effects is not included in this report.

Also possible are decreases in thermal conductivity resulting from the incorporation of TRU into the fuel. For example, Fig. 3.2 shows a plot of the thermal conductivity of americium oxide relative to other actinide oxides. Reduction of fuel thermal conductivity would result in increased fuel temperatures and consequently increased gas release.

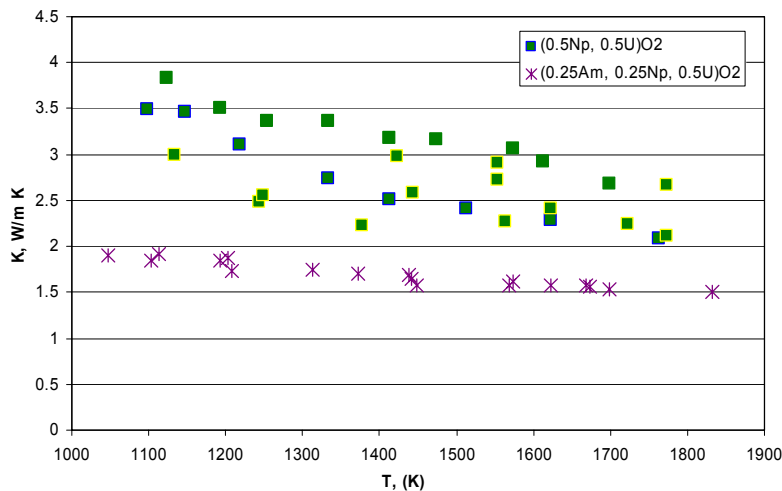


Figure 3.2. Thermal conductivity of Am-bearing oxide fuels relative to U, Pu, and Np oxide fuels. Data: Babelot, JRC-ITU-TN-99/03 (1999)

4.0 FUEL MODELING

4.1 Pin-type fuel

Fuel behavior during core accident conditions drives GFR fuel design. During normal operation, core coolant pressure (7 MPa) offsets cladding tensile hoop stress generated due to fission gas pressurization of the fuel pin. This results in low tensile hoop stress (or compressive stress) in the cladding during normal operation. GFR loss-of-coolant pressure accidents, however, are severe in terms of negative consequences to the fuel. Loss of coolant pressure coupled with a core temperature rise and increased fission gas release results in a large increase in pin internal gas pressure. This increase in internal pressure, coupled with a decrease in external cladding restraint due to depressurization results in a large increase in cladding hoop stress. For metal cladding, this increase in stress is concomitant with a decrease in cladding creep strength due to increased cladding temperature. This scenario results in the potential for a high probability of massive failure of fuels that are conventionally clad in sealed pins. The introduction of americium into the fuel exacerbates this issue by increasing fuel pin gas inventory, leading to yet higher pin failure probability.

Fuel pin models that capture the effect of additional gas inventory due to americium on cladding stress can be easily implemented using spreadsheet calculations and/or finite element analysis. Prediction of failure probability is, however, difficult due to the lack of high-temperature irradiation creep data germane to the cladding systems of potential interest. These include Nb-based refractory alloys, ODS alloys, SiC composites, and duplex cladding systems. Tables 4.1 and 4.2 and Figure 4.1 provide examples of the hoop stress introduced during a loss-of-coolant scenario for a sealed fuel pin originally operating at an average plenum temperature of 650°C at and a burnup level of 10 at.% prior to core depressurization followed by a temperature rise to 1600°C. The specific correlations applied to calculate fission gas and helium release from the fuel are the same as those used in section 4.2. Because the fuel is designed to allow pellet to cladding mechanical contact only at end-of-life to prevent fuel-cladding-mechanical-interaction, cladding stress, and thus cladding lifetime, are driven by gas pressure. Cladding stress can be manipulated by varying the fuel to gas plenum volume ratio.

Table 4.1 shows data for a fuel to plenum length ratio of 1:1. It can be seen that under normal reactor operating conditions, the cladding is in compression, and cladding creep-down becomes a potential issue. This is also a phenomenon of concern in pressurized light water reactors, and is addressed by pre-pressurizing the fuel pins with helium gas during fabrication. LWR fuels, however, typically have very low gas release relative to fast reactors due to lower power density and peak fuel temperature. They do not, therefore, tend to exhibit the wide swings in pin internal pressure characteristic of fast reactor fuels operating at much higher power density and temperature. The higher gas release rates and the nature of the core depressurization accident make the use of pre-pressurized fuel pins problematic for the GFR.

The data in Table 4.1 show that the consequences the core depressurization overwhelm the effects due to americium below about 5% Am (percent of heavy metal). At 5% Am, additional gas inventory has a significant impact on cladding hoop stress, increasing cladding stress by approximately 25%. At 20% Am, the cladding stress more than doubles during accident scenarios relative to the case of no americium. The assumed cladding transient stress limit of 20 MPa (2900 psi) for short times at high temperature (1600°C) cannot be met for any fuel design using a short plenum.

Table 4.1. Example of increase in cladding hoop stress for a (U,Pu)N fuel during postulated core depressurization accident conditions. The fuel to plenum length ratio is modeled as 1:1.

Condition	Cladding hoop stress (MPa)
10% burnup, no Am, normal operation at 8 MPa, 650°	-18.7 (compressive)
10% burnup, no Am, atmospheric pressure, 1600°C	35.6
10% burnup, 2.5% Am, atmospheric pressure, 1600°C	40.5
10% burnup, 5% Am, atmospheric pressure, 1600°C	45.3
10% burnup, 10% Am, atmospheric pressure, 1600°C	55.1
10% burnup, 20% Am, atmospheric pressure, 1600°C	74.5

Table 4.2 shows data for a plenum to fuel length ratio of 2:1. In this scenario, the cladding transient stress limit can be met for americium levels up to about 2%. A plenum to fuel length ratio of 4:1 would be required to accommodate 20% Am in the fuel. In other words, only 20% of the length of the cladding tube would contain fuel. Smaller plena are required in liquid metal-cooled systems due to the less demanding nature of anticipated transients.

Table 4.2. Example of increase in cladding hoop stress for a (U,Pu)N fuel during postulated core depressurization accident conditions. The fuel to plenum length ratio is modeled as 2:1.

Condition	Cladding hoop stress (MPa)
10% burnup, no Am, normal operation at 8 MPa, 650°	-20.7 (compressive)
10% burnup, no Am, atmospheric pressure, 1600°C	18.6
10% burnup, 2.5% Am, atmospheric pressure, 1600°C	21.1
10% burnup, 5% Am, atmospheric pressure, 1600°C	23.7
10% burnup, 10% Am, atmospheric pressure, 1600°C	28.8
10% burnup, 20% Am, atmospheric pressure, 1600°C	39.0

Increasing the fuel plenum length has the consequences of increasing pressure drop across the core and requiring a much longer core pressure vessel. It may also result in pin vibration issues. The practical limit on plenum to fuel length ratio has not been determined, but is likely to be on the order of 2:1. This would indicate that americium contents on the order of 5 at.% are likely to be possible for this type of fuel.

Due to the nature of the GFR depressurization accident and the consequent need for large gas plenums to prevent massive pin failure, GFR designs of the 1970's tended toward the use of vented fuel pins as a solution to this issue. Vented pin concepts typically use a long diffusion path length coupled with carbon 'traps' or 'filters' to allow the fuel pins to breathe while preventing newly formed fission product release to the core coolant. Pin internal and external pressures are essentially equal, resulting in no net cladding hoop stress and no possibility for gas-driven creep rupture of the fuel pins. Vented pins offer a solution that would be immune to the effects of additional helium gas production due to the minor actinides. These concepts are difficult to implement in practice, however, resulting in some degree of increased cost and complexity relative to sealed pins.

Another potential alternative would be to vent fuel pins through a rupture disk during accident conditions. During normal operation, a plenum to fuel ratio of 1:1 or less would be sufficient to ensure that cladding stress remains at a low level. During a high-temperature excursion, a 'rupture disk' fitted to the pin would be designed to release gas to the coolant only when the pin internal pressure rises beyond the rupture disk pressure limit. This would prevent potential flow blockage issues due to 'ballooning' of the cladding from arising during accident conditions. Use of this concept would likely result in a decrease in fuel reliability during normal operating conditions, however.

Modeling of vented fuel concepts offers no additional insight into the behavior of fuels with high minor actinide content, since the principal difficulties with this concept are design interface issues. The life limiting factor for the fuel shifts from internal pressurization to an issue such as cladding corrosion or pellet-cladding-mechanical-interaction, which is not yet obvious.

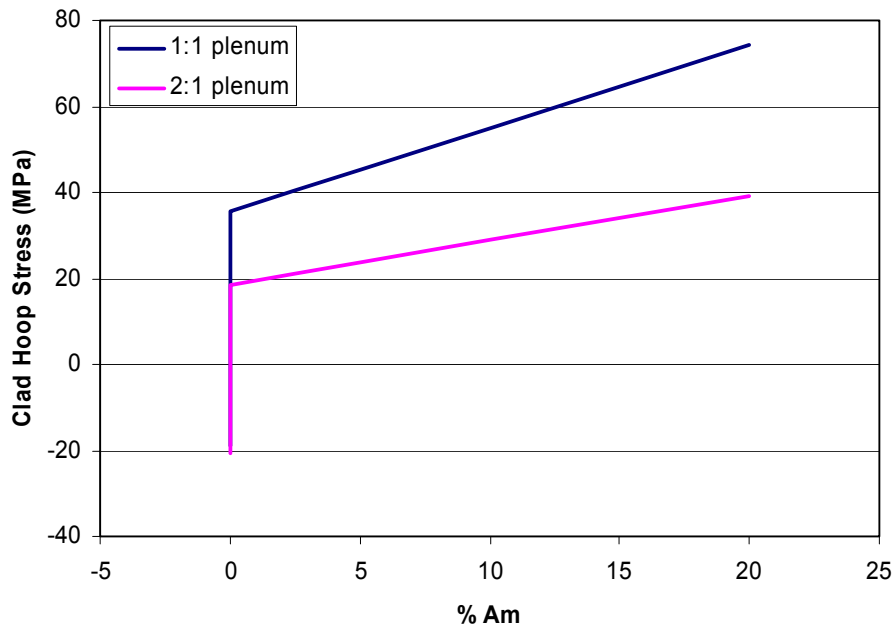


Figure 4.1. Response of cladding hoop stress to GFR accident conditions

4.2 Unrestrained particle fuel model

The behavior of beds of fuel particles were modeled as single spherical fuel particles surrounded by a thick-walled pressure vessel. Gas pressure in the sphere generates a stress in the sphere wall, which can be compared as a function of particle size, americium content in the fuel, and buffer and coating thickness.

The fission gas release rate from the fuel particle was calculated by a best-fit correlation equation from UN fuel data

$$R = 100/[\exp(0.0025\{90TD^{0.77}/B^{0.09} - T\}) + 1] \quad (\text{eqn. 4.1})$$

where TD is the fraction of theoretical density, B is the burnup fraction and T is the absolute temperature. [63] The helium release rate from the fuel particles was taken as five times the fission gas release for this investigation. The 5:1 ratio is a conservative value based on results of the EFTTRA-T4 test (see section 3). Released fission gas and helium are assumed to expand into pores within the fuel particle and buffer layer, which generates pressure inside of the hollow sphere of matrix material. The pressure is calculated using the ideal gas law. The stresses at a distance, R, from the center of a thick-walled pressure vessel in spherical coordinates are given by:

$$\sigma_R = \frac{p_i a^3 (b^3 - R^3)}{R^3 (a^3 - b^3)} \quad (\text{eqn. 4.2})$$

$$\sigma_\theta = \sigma_\phi = \frac{p_i a^3 (2R^3 + b^3)}{2R^3 (b^3 - a^3)} \quad (\text{eqn. 4.3})$$

where p_i is the internal gas pressure, a is the inner radius of the matrix shell, b is the outer radius of the matrix shell, and R is the radial distance within the shell. [64] The stresses are dependent on the location within the shell matrix and reach a maximum at the inner shell radius and then decrease to a minimum at the outer shell radius. In this way, stress in the particle shell can be easily calculated.

Figure 4.2 shows plots of stress in the shell of a particle with the attributes given in Table 4.3

Table 4.3. Attributes of modeled fuel particles

Parameter	Value
Fuel type	(U,Pu,Am)N
Kernel diameter	1 mm
Kernel density	85% theoretical
Buffer layer thickness	48 μm
Buffer layer density	50% theoretical
Buffer layer composition	Low-density TiN
Outer shell thickness	100 μm
Outer shell composition	Dense TiN

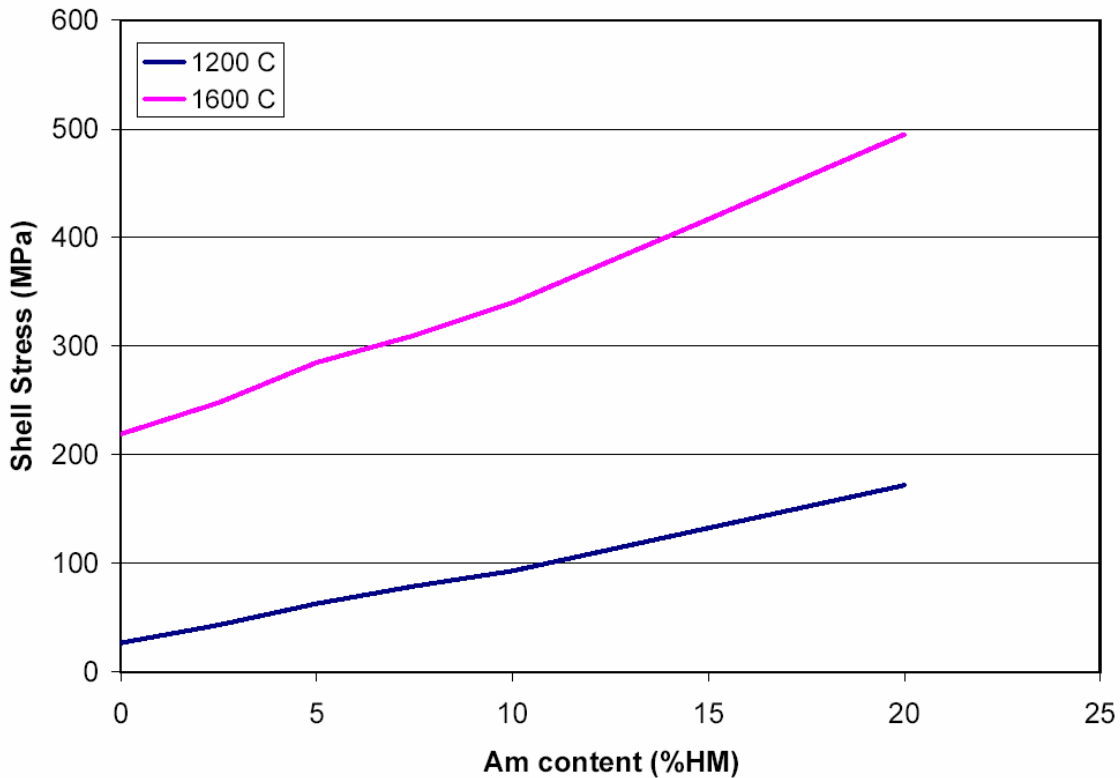


Figure 4.2 Effective stress on outer shell of fuel particle as a function of Am content at 1200° and 1600°C and 10% burnup.

Because the particle packing density is low and all fission gas must be accommodated internally in a ‘buffer layer’ (effectively a gas plenum), fuel particle coating layers must be very thin relative to those used on TRISO fuel. As a result, it can be seen from Fig 4.2 that high stresses are generated in the fuel particle shell wall under core accident conditions for even for fuels with no americium content. Analysis of the failure probability of ceramic fuel particles should be done using a classic Weibull type analysis

based on failure statistics. As with all GFR fuel concepts, the lack of a suitable statistical database for chemically vapor deposited titanium nitride (CVD-TiN) prevents a quantitative assessment of failure probability under these conditions. Typical strengths for monolithic nitride ceramic materials are on the order of 400-600 MPa, however. If a 'factor of safety' of ~5X less than fracture stress under accident conditions is applied (100 MPa peak stress at 1600°C, as used for dispersion fuel matrix stress limit), then it is clear that this concept is marginal at the target burnup level of 10 at.% without the incorporation of americium. Incorporation of Am further decreases the probability that this fuel concept can be successfully implemented for MA management.

4.3 Dispersion fuel model

Because of the complex microstructure of dispersion fuels, two separate finite element models are required to gauge fuel performance. An element scale model containing all of the microstructural features of a dispersion fuel (millions of particles, hundreds of millions of nodes) would be far too computationally intensive for practical application as a screening tool. Instead, a macroscopic model with no microstructural detail is used to calculate macroscopic thermal stresses and fuel temperatures. A micro-scale model is then used to calculate the local stress state of the fuel element due to gas pressure and fuel particle swelling as a function of americium content. Fuel to coolant ratio was kept constant at 50 vol.% for all concepts. Fuel particle loading was also fixed at 50 vol.%.

4.3.1 Macroscopic stress model

Hexagonal block fuel elements were modeled using two different size concepts, with 1 cm and 15 cm side lengths. The 1 cm side length (1.73 cm flat to flat) hexagonal elements represent the thermal gradients and stresses present in a dispersion fuel element consisting of small diameter pins that are bundled together to form an assembly. The larger element (15 cm side length, 25.98 cm flat-to-flat length) represents fuel elements for a core similar to a GT-MHR, where blocks are stacked in a hexagonal array. Both sizes of fuel elements were modeled using a 1/6 segment representation of a hexagonal element as shown in Figure 4.2 as well as full-scale six-sided element models. Elements with hexagonal and cylindrical flow channels were modeled to gauge the effect of flow channel geometry on macroscopic thermal stresses within the fuel.

Multiple models were drawn with various numbers of cylindrical flow channels. To simulate helium coolant flow, a convection coefficient of 1500 W/m²·K was applied to the surfaces of the flow channels and along the outer edge of the fuel element model. A constant uniform heat generation rate of 2.0x10⁶ W/m³ was applied to the solid homogeneous fuel matrix to model the volumetric heat generation due to fission. At a constant coolant volume fraction of 0.5, this results in a core power density of 100 MW/m³ at the location of the analysis. An average ambient gas temperature of 650 °C used in the model calculations. Table 4.2 contains the material properties assumed for the FEA models. The FEA models were used to complete steady-state thermal and static stress analysis. A typical fuel element model contained 100,000 – 200,000 nodes. To obtain stress contours, models were analyzed without physical constraints to motion,

simulating a free floating block or pin. Hand calculations of strain due to thermal expansion were used to verify the adequacy of the model in calculating thermal strains.

Table 4.4 Parameters for global FEA model

Coolant temperature	650°C
Fuel thermal conductivity (W/m*K)	15
Heat generation (W/m ³)	2.00E+06
Convection coefficient (W/m ² *K)	1500

4.3.1.1 *Small element with hexagonal flow channels*

All models of pin-type fuel with hexagonal flow channels had a 1 cm side with a 1.73 cm flat to flat dimension. Computational data acquired from the hexagonal models is shown in Table 4.5. Figure 4.3 shows a typical stress plot of a fuel model with hexagonal coolant channels. Note that the temperature gradient is less than 10°C across the element. To maintain a uniform web thickness throughout the entire element and reduce stress concentrations, coolant flow channels were cut from outer edges of the elements. Slightly lower stresses result from models that incorporate coolant channels into the outer edge of the element, and a further slight reduction in stress results from fillets to the corners of the coolant channels. In all cases, stress levels are low and acceptable relative to the known properties of SiC. Fuel temperatures remain low, peaking at approximately 100°C above the coolant temperature.

Table 4.5. Temperature and stress data for 1.73 cm diameter hexagonal fuel pin with hexagonal flow channels

No. of Channels	Max Temp (°C)	Max Stress (MPa)
61 (straight)	696.8	4.1
61 (coolant channels at element edges)	695.8	3.6
61 (channels at edges & fillets at corners)	697.5	3.4

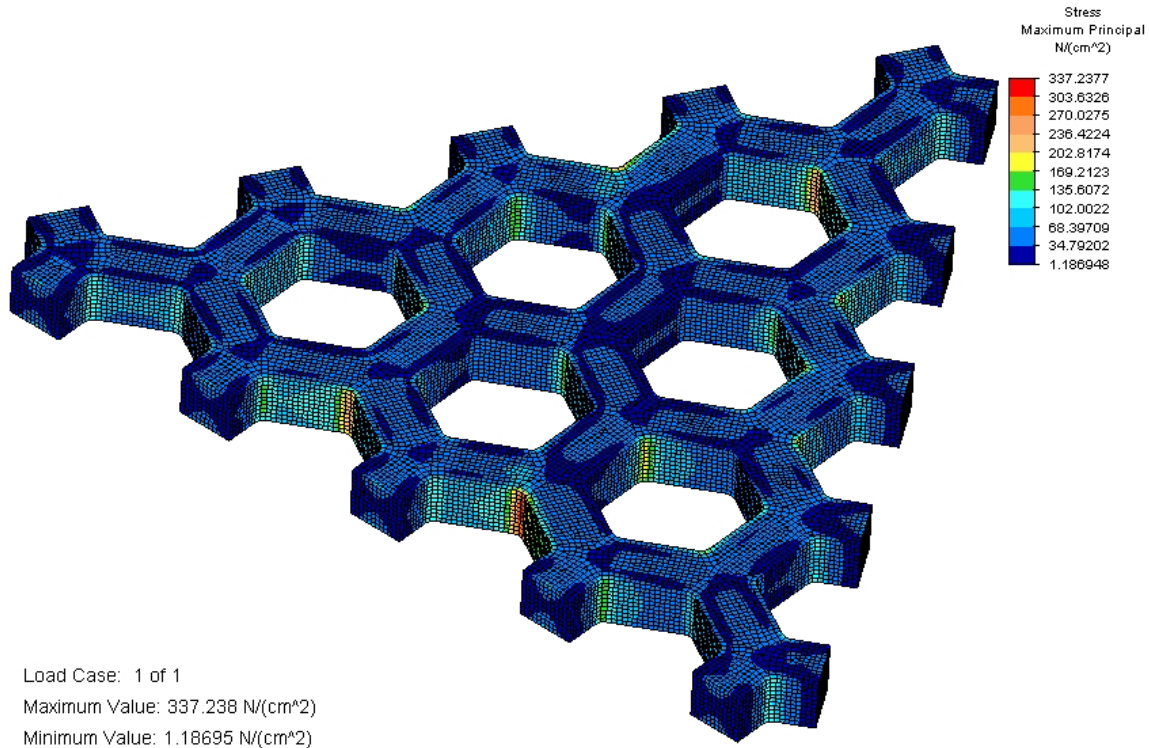


Figure 4.3. Stress plot of 1.73 cm (flat-to-flat) hexagonal fuel element with hexagonal coolant channels.

4.3.1.2 Small element with cylindrical coolant flow channels

Table 4.6 summarizes calculational data obtained from the analysis of small GFR fuel elements with cylindrical flow channels. Elements have a 1.73 cm flat-to-flat dimension, and would be bundled to form an assembly. As in the case of the elements with hexagonal flow channels, the diameter of the channels was varied for while the fuel/coolant fraction was held to 50% in order to generate parametric data.

Figure 4.4 shows the steady state thermal analysis results obtained from modeling a hexagonal fuel element model with a side length of 1 cm and containing 91 cylindrical coolant channels. The diameter of the cylindrical channels is 1.35 mm resulting in a web thickness is 0.431 mm. Table 4.6 gives further results for models with fuel channel diameters ranging from 1.1 – 3.0 mm. Fuel temperatures are in the range of 685 - 738°C resulting in peak maximum principle stresses of 2.7 – 5.9 MPa, negligible values considering the strength of SiC.

Fabrication difficulties would likely dominate the practical utility of these small elements, due to the many small coolant channels that would have to be introduced into a long, spaghetti-like ceramic element, although elements with cylindrical flow channels are likely to be more practical from the standpoint of fabrication than elements with hexagonal flow channels. An alternate design not yet modeled would incorporate fewer coolant channels and a slightly larger element diameter.

Table 4.6. Temperature and stress for small scale elements with cylindrical coolant channels.

No. of coolant channels	Channel diameter (cm)	Web thickness (cm)	Max Temp (°C)	Max Stress (MPa)
19	0.2950	0.0875	738.3	5.9
37	0.2114	0.0650	713.5	4.5
61	0.1647	0.0518	700.6	3.9
91	0.1348	0.0431	692.6	3.4
127	0.1141	0.0369	685.9	2.7

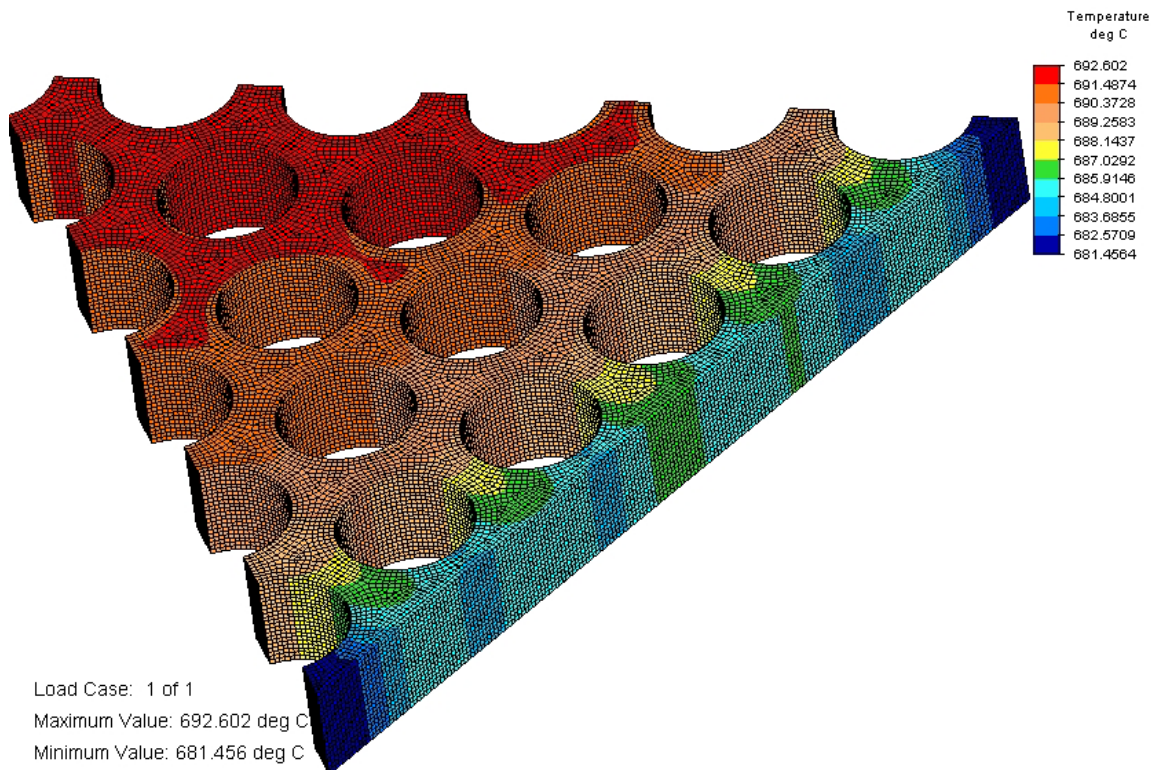


Figure 4.4. Thermal model (1/6 element) of 1.73 cm (flat-to-flat) hexagonal fuel element containing 91 cylindrical coolant channels.

4.3.1.3 Large block-type fuel with cylindrical flow channels

Hexagonal block-type fuel were modeled as 1/6 segment models for a variety of coolant channel diameters. These elements would be stacked together to form a core similar to the manner in which HTGR elements are assembled. The temperature gradients and stress in the larger block-type fuels are significantly increased relative to the smaller ‘pin-like’ fuels. Larger web thicknesses result in higher peak temperatures and temperature gradients, which result in higher peak stress values as the cylindrical channel diameter increases. Figures 4.5 and 4.6 plot the relationship between the circular coolant channel diameter and the fuel element maximum temperature and the coolant channel diameter and fuel element maximum principal stress for a 1/6 element hexagonal model. Elements modeled with coolant channel diameter less than 1 cm exhibit maximum principal stresses of less than 150 MPa. Maximum element temperature is approximately 1000°C for 15 cm diameter plates with 1 cm diameter channels.

Based on the results of the 1/6 element hexagonal model, full hexagonal fuel element models were used to further analyze fuel temperatures and the macroscopic thermal and stress distribution across a whole element. Figure 4.7 is an image of the calculated temperature distribution in a full hexagonal model. The steepest temperature gradients, and hence the largest thermal stresses occur at the 6 corners of the hexagon due to ‘over cooling’ of these areas relative to the remainder of the fuel element. To eliminate these areas of high stresses, this material was removed by cutting a 60° wedge of material including the high stress volume from the corners of the hexagon. Figure 4.8 shows that this reduced the stress significantly in these locations, however the location of the peak stress remains in the near surface region of the coolant channels nearest the six corners of the element.

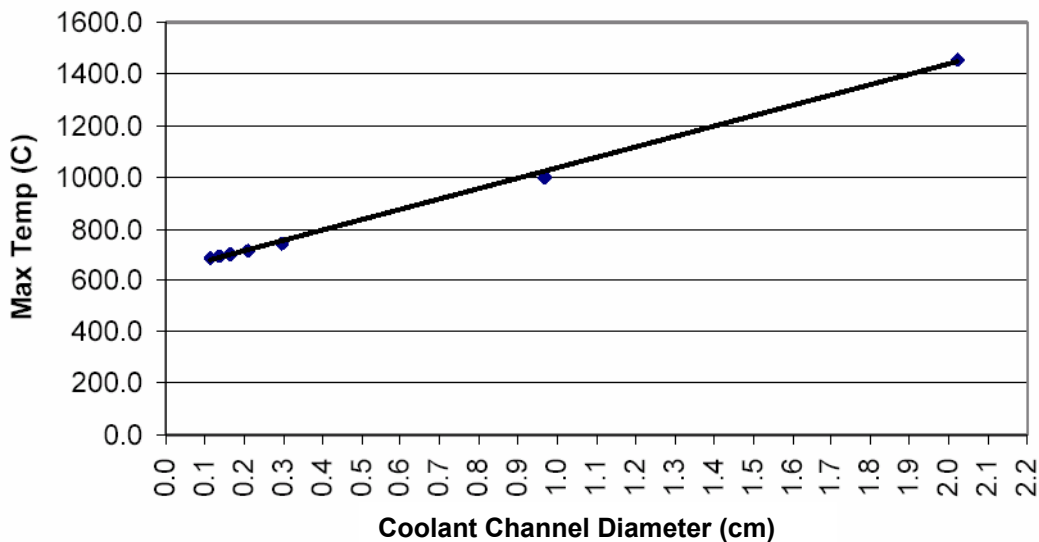


Figure 4.5. Maximum temperature in a ‘full’ hexagonal fuel model as a function of coolant channel diameter.

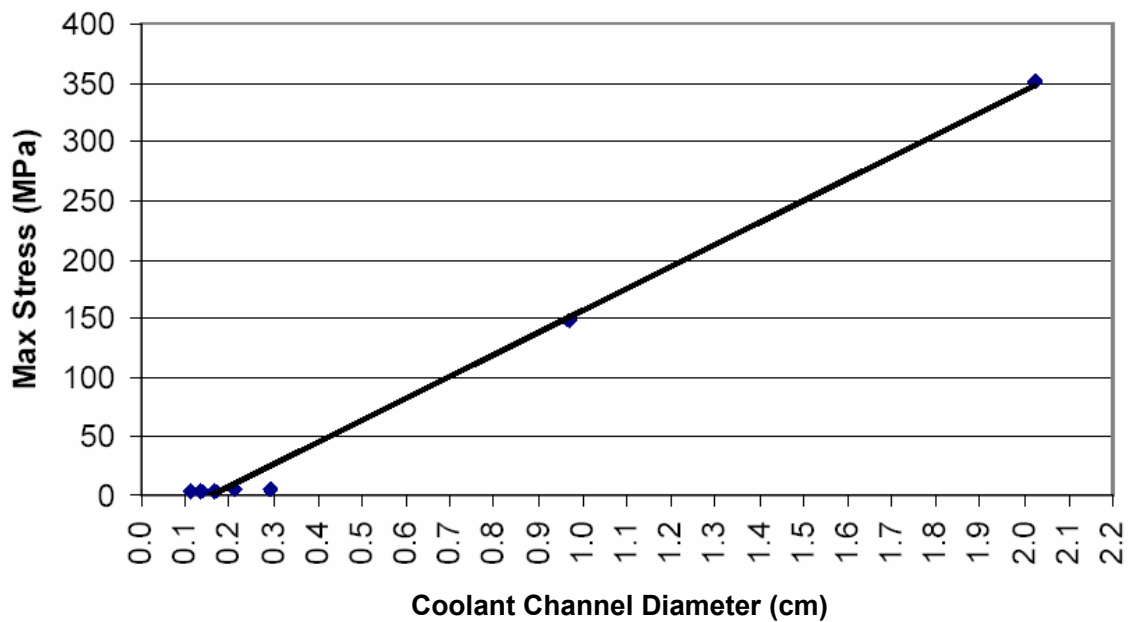


Figure 4.6. Maximum stress in ‘full’ hexagonal fuel elements as a function of coolant channel diameter.

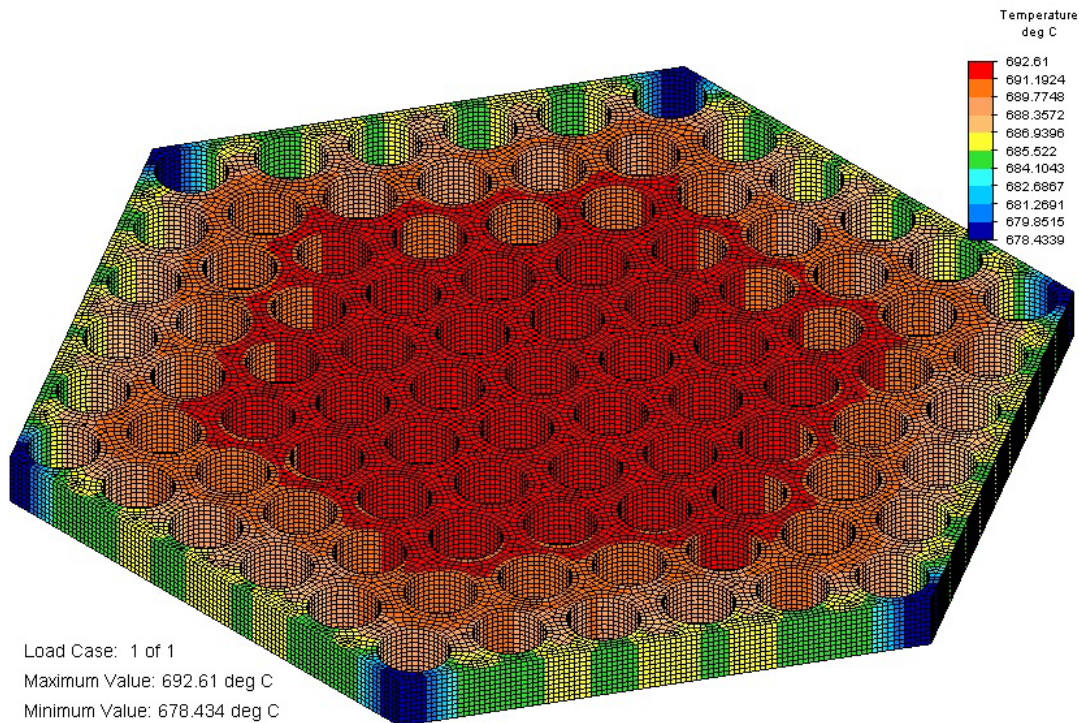
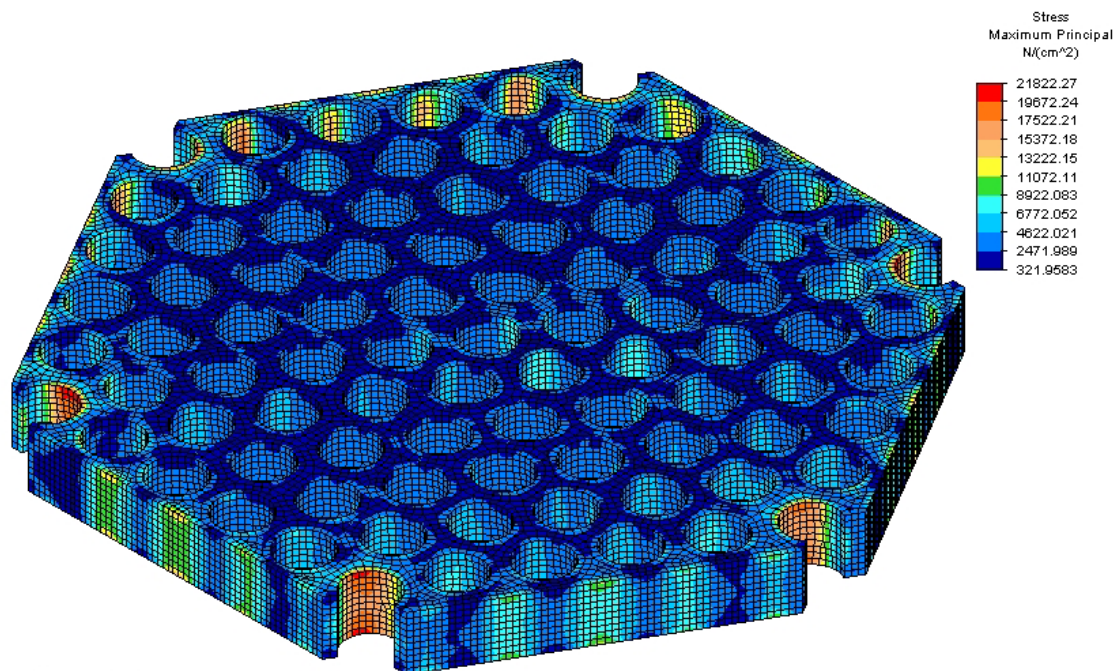


Figure 4.7. Temperature plot of ‘full’ hexagonal fuel element showing largest thermal gradients at the corners of the model (geometry a). 1 cm edge length shown.



Load Case: 1 of 1
 Maximum Value: 21822.3 N/(cm²)
 Minimum Value: 321.958 N/(cm²)

Figure 4.8. Stress plot of ‘full’ hexagonal element model with corners removed to reduce stress in these areas (geometry b). 1 cm edge length shown.

Table 4.7 lists peak temperature and peak maximum principal stress data for full hexagonal fuel element models of differing edge lengths each with 91 cylindrical coolant channels. Data is shown for models with and without modifications to the geometry to reduce stress discussed above; model geometry ‘b’ denotes removal of material at the corners of the hexagon. Results from the hexagonal (full) model indicates that coolant channel diameters of less than 1 cm are required in order to maintain thermal gradients and consequent steady state thermal stresses at a reasonable level.

Table 4.7. Summary of maximum element temperature and stress for full hexagonal models with varying coolant channel diameters.

Coolant channel diameter (cm)	Model geometry	Max Temp (°C)	Max Stress (MPa)
0.27	a	692.6	23.2
0.27	b	694.3	13.5
1.0	b	1060.5	218.2
2.0	a	1535.1	1044.2
2.0	b	1604.2	607.9

The large increase of stress calculated for the full hexagonal block model relative to the 1/6 element model requires further design improvement to further decrease the steady state thermal stress. Smaller diameter high aspect ratio elements bundled into a fuel assembly offer a potential alternative design that operate at a lower temperature, lower temperature gradient, and consequently a much lower internal stress level.

4.3.2 Micro-scale modeling of GFR dispersion fuel

Due to the complex geometry and stress state within the matrix of a dispersion fuel, an analytical solution for stress state is not possible. Finite element modeling was therefore used to assess the state of stress and to make judgments about the relative impact of americium on the stress within a dispersion fuel matrix.

4.3.2.1 Description of micro-scale model

Dispersion fuel was modeled as an array of spherical fuel kernels embedded in a SiC matrix which acted as a pressure vessel with variable thickness walls. Fuel particle volume fraction was kept constant at 0.5. Stress in the matrix was calculated on the basis of fuel swelling and gas release from the fuel as a function of burnup, temperature, and americium content. Thermal gradients and resulting thermal stresses were calculated using FEA and found to be negligible on the scale of this model and were therefore ignored.

The modeled fuel was roughly equivalent to the reference design in Table 2.7, except that a mono-modal kernel size distribution was used. The cavity in the matrix includes the UC spherical kernel and the coating used as a buffer between the fuel and the matrix. The reference design calls for a low density SiC buffer which was modeled to have 50% porosity. The initial volume in the cavity available for gas expansion thus consists the 50 vol.% void space in the buffer along with the 15 vol.% void space within the volume of an 85% dense (U,Pu)C kernel.

The release rate for fission gas into the dispersion cavity was based on data from carbide pellet type fuel shown in Fig. 4.9. Results from U.S. experiments on gas release from fuels with low oxygen content indicate (conservatively) a linear release of 2% per atom percent burnup beyond a threshold burnup value of 3 at.%. Helium gas generation was estimated at 50 ml/g of ^{241}Am transmuted based on the analysis of available data in Section 3.

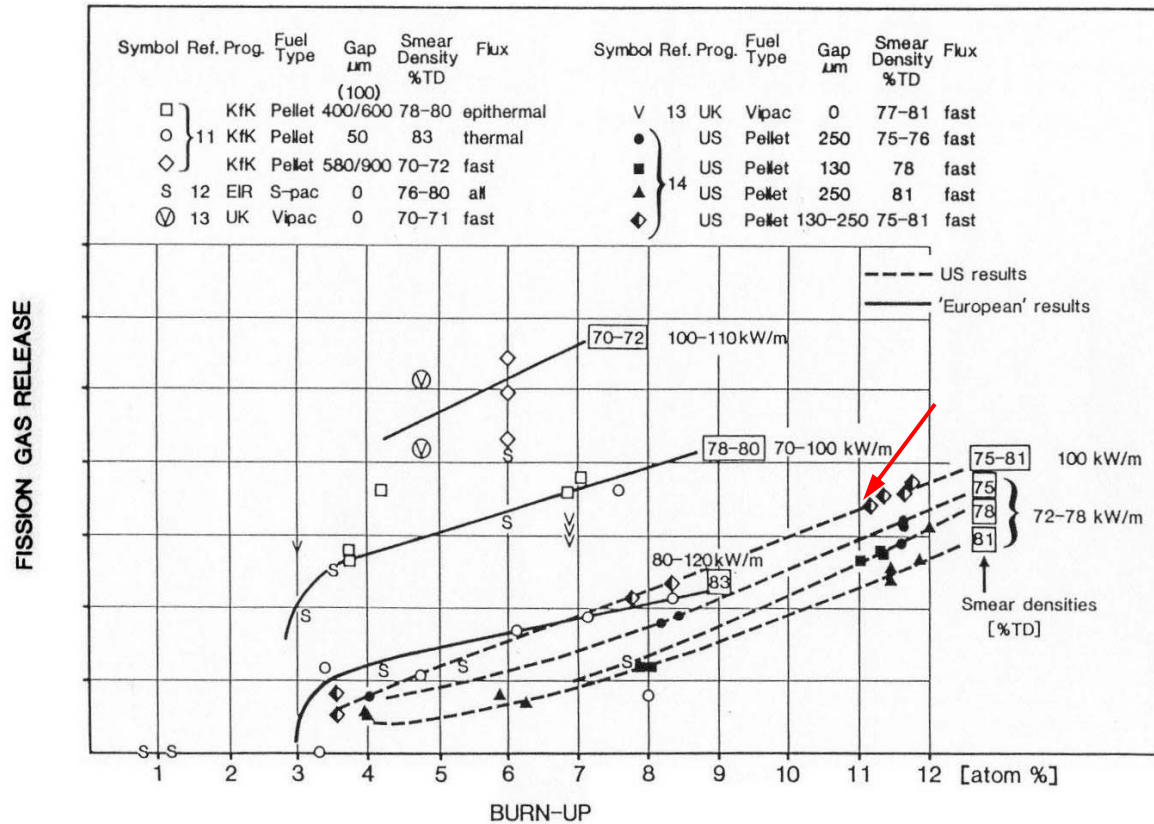


Figure 4.9. Gas release data for carbide fuels. Gas release for dispersion fuels was modeled as 2% per at.% burnup beyond a burnup threshold of 3 at.%. This is a conservative value based on data from U.S. fuels with low oxygen content.

Two models were investigated for modeling the matrix stress; a 3 x 3 x 3 cubic structure consisting of 27 total kernels (Fig. 4.10) and a smaller model consisting of only 4 kernels. The smaller 4 kernel model gave results consistent with the 27 sphere model, and was more manageable in terms of computational resources. Fig. 4.11 shows an example of the representation of stress output from the 4 kernel model. Here the model has been sliced at the midplane to show internal stress. Peak stresses that occur on the edges of the models are due to asymmetry at the model boundary and are ignored. The peak stress relevant to fuel performance determination occurs in the thin web of matrix material located between adjacent particles. The maximum value of principal stress always occurs at this point and was used as an indicator of the response of the matrix stress to increasing americium content.

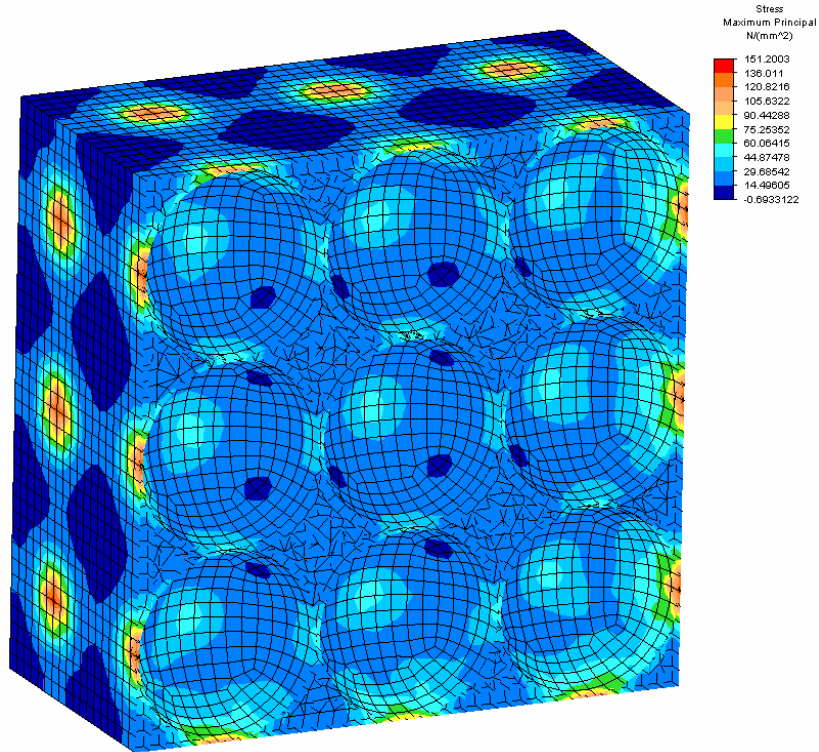


Figure 4.10. Cross-section of 27 cell dispersion fuel model.

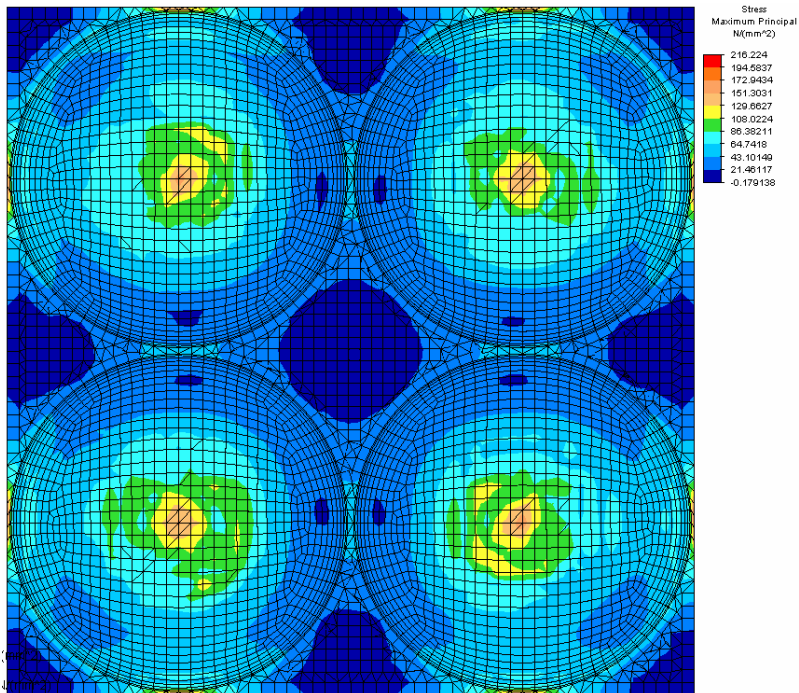


Figure 4.11. Example of stress results from 4 cell dispersion fuel model

4.3.2.2 Results of micro-scale modeling of dispersion fuel

The 4 kernel micro-scale model was used to perform matrix stress analyses at 3 different fuel temperatures (800 °C, 1200 °C, and 1600 °C) and americium contents ranging from 0-10 at.% of heavy metal. Fig. 4.12 provides an example of the evolution of matrix stress as a function of burnup for americium contents of 0-10 at.% (percent heavy metal) at 1200°C. Matrix stress increases approximately in an exponential manner with burnup, as total gas inventory and gas release rate increase and fuel kernels swell to fill the space available for gas expansion. Assuming a low modulus buffer layer, no fuel particle to matrix contact occurs below 10 at.% burnup.

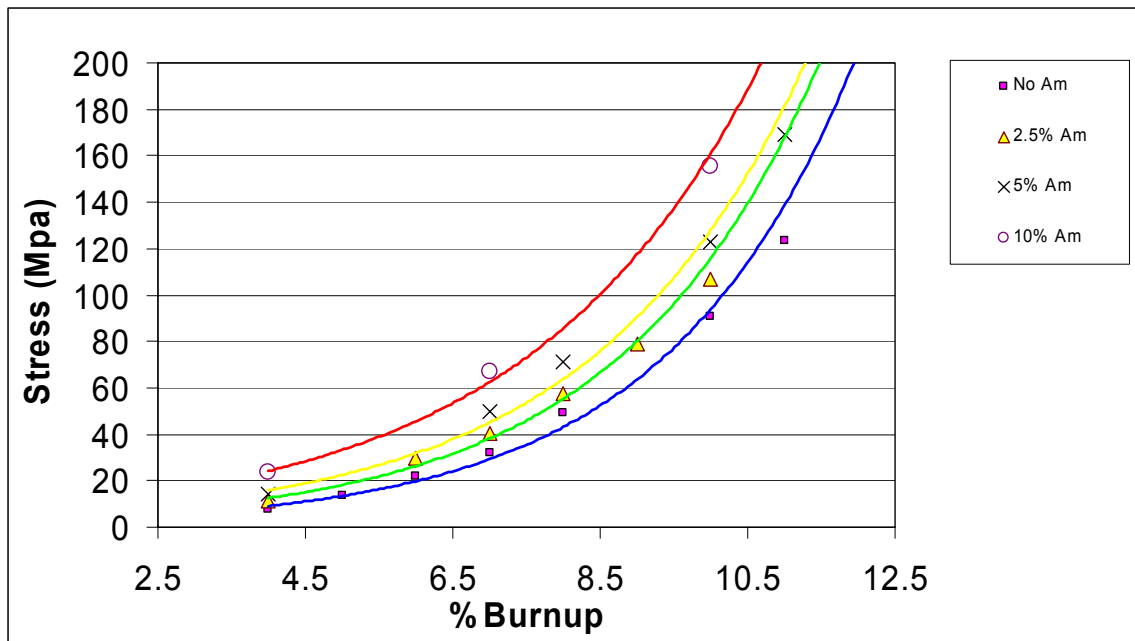


Fig. 4.12. Evolution of matrix stress for dispersion fuel at 1200°C.

Plots of the evolution of stress as a function of temperature for 4, 7, and 10 at.% burnup are shown for americium levels of 0, 2.5, 5, and 10 at.% in Figs. 4.13 – 4.16. These plots provide an indication of how matrix stress evolves as a function of temperature and burnup for each case.

The strength of brittle materials (materials with low fracture toughness), such as ceramics, is heavily dependent on the density, size, and location of microstructural irregularities (flaws) in the material. These flaws are invariably introduced during the fabrication process. A rigid analysis of failure probability would require a statistical database consisting of test data for the material being analyzed. The strength of these materials depends not only on the type of manufacturing process used, but also on the geometry of the component (volume under stress) and the specifics of the process, such as origin and impurity levels of feedstock. In the absence of such a statistically significant

database, it is thus very difficult to judge strength limits and failure probability. Rough assumptions are thus used to gauge the likelihood of failure.

Well made SiC monoliths have typical 4-point bend strength values in the 400-500 MPa range. Applying conservatism leads to consideration of an allowable stress limit of 100 MPa. It must be stressed that this is currently an arbitrary limit, put forth more as a value for comparison of the various cases.

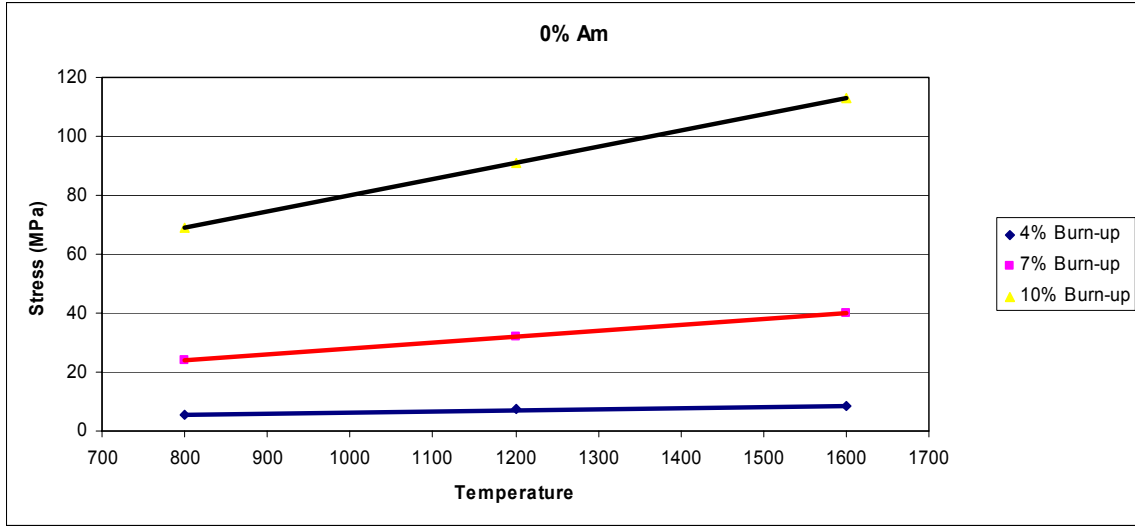


Fig 4.13. Matrix stress as a function of temperature for fuel containing no americium at 4, 7, and 10 at.% burnup.

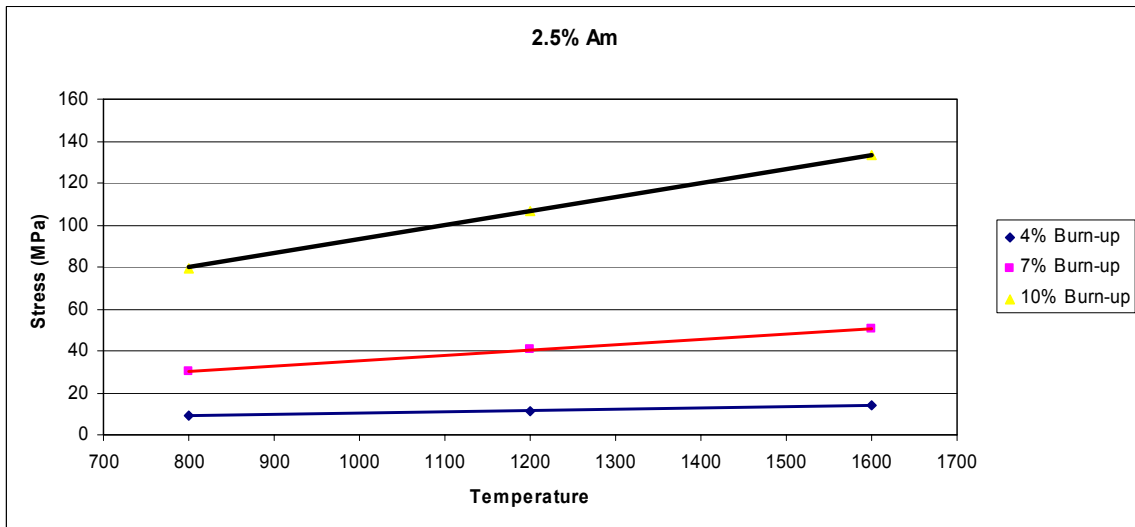


Fig 4.14. Stress as a function of temperature for fuel containing 2.5 at.% americium at 4, 7, and 10 at.% burnup.

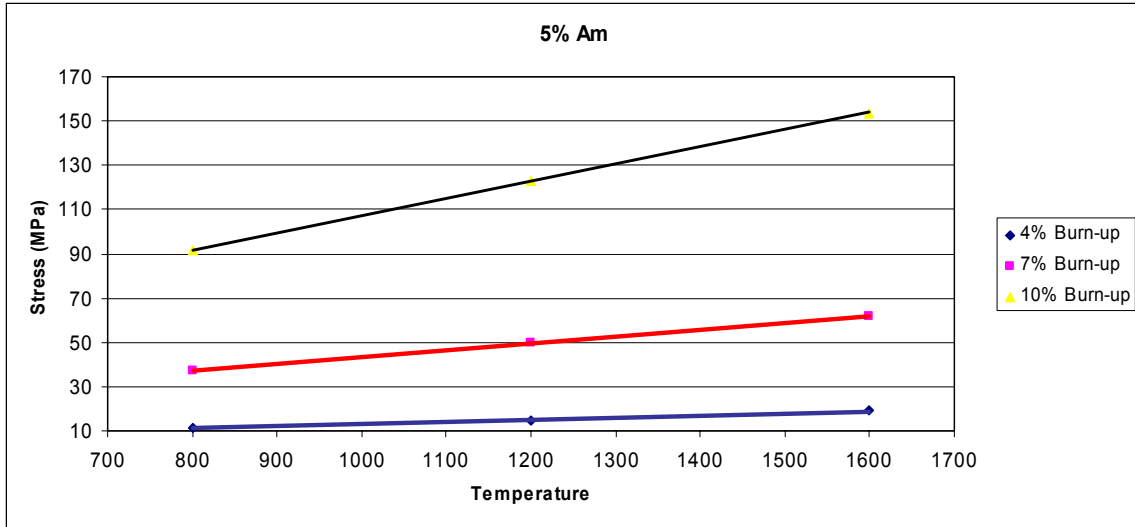


Fig 4.15. Stress as a function of temperature for fuel containing 5 at.% americium at 4, 7, and 10 at.% burnup.

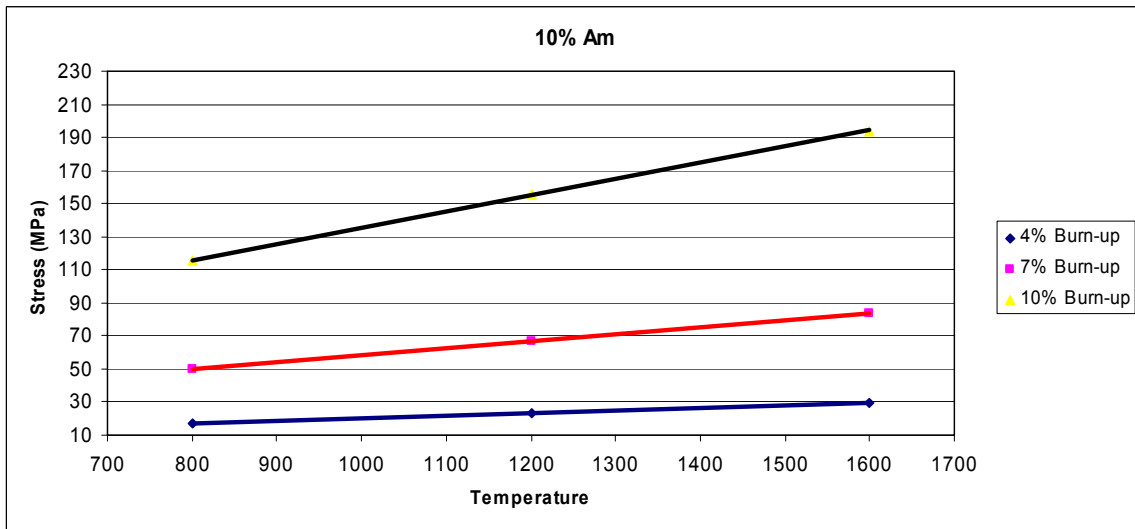


Fig 4.16. Stress as a function of temperature for fuel containing 10 at.% americium at 4, 7, and 10 at.% burnup.

As can be seen in Figs. 4.13-4.16, the increase in stress is linear with temperature, since for these cases no temperature dependence of the gas release rate was assumed. Typically, gas release rate increases with temperature, and would result in non-linearity of these plots, however the existing database for carbide fuels did not support such assumptions.

First considering the case of no americium, it can be seen that at an assumed fuel operating temperature of 1200°C, the modeled matrix maximum principal stress levels remain below the 100 MPa target limit for fuel burnup beyond 10 at.%. The spacing of the plotted lines indicates the exponential increase in stress with burnup, as discussed above. The addition of 2.5 at.% Am increases the stress in this case (1200°C and 10 at.% burnup) by approximately 18% relative to the case with no americium. This results in a decrease in burnup potential of approximately 0.6 at.%, assuming that the matrix stress level chosen is a valid indicator of fuel burnup limit. Likewise increasing the Am content to 5 and 10 at.% results in a matrix stress increase of 36% and 71% respectively. Since stress increases exponentially with burnup, when the 100 MPa reference stress limit is applied, decreases in burnup limits of 1.1% and 1.6 at.% result.

Also significant is the behavior of the calculated matrix stress during the 1600°C transient case. Fig. 4.17 shows calculated matrix stress as a function of burnup for americium contents of 0-10 at.% heavy metal at 1600°C. Here the reference stress of 100 MPa is exceeded at about 7.5 at.% burnup for an americium content of 10 at.%. For the case of fuel with no americium, the 100 MPa limit is reached at 9.7% burnup. The intermediate case (5 at.% Am) reached 100 MPa at approximately 8.5% burnup, a decrease of slightly over 1% relative to the case with no americium.

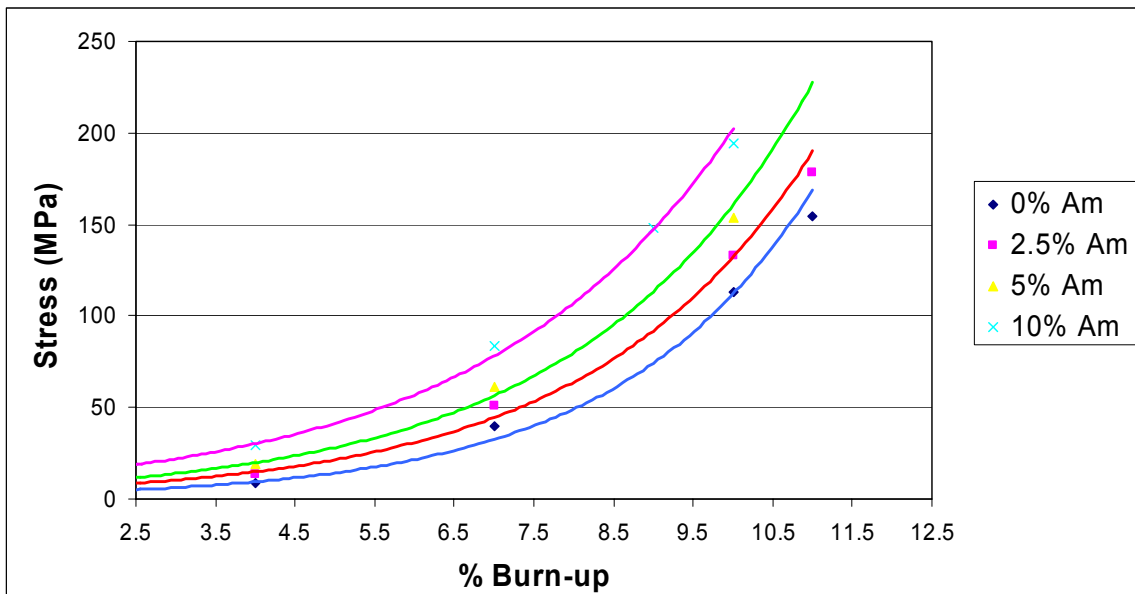


Fig 4.17. Evolution of matrix stress as a function of burnup at 1600°C for americium contents of 0-10 at.%.

The results of this analysis indicate that americium contents on the order of 5 at.% result in some potential loss of margin under GFR accident conditions, but are in general acceptable. Burnup limits determined on the basis of core accident behavior can be expected to be approximately 1-2% lower than for a fuel containing no americium.

5.0 SUMMARY

In large part, the feasibility of the GFR for minor actinide burning depends on the limitations of the fuel. GFR fuel concepts represent a compromise between heavy metal density and the ability to withstand GFR severe accident conditions. Two fuel types appear most likely to meet GFR design goals; these are pin-type refractory ceramic fuels clad with refractory materials and dispersions of refractory particles in a refractory matrix. Both fuels require extensive research before a definitive feasibility judgment can be made, and extensive development and qualification prior to implementation.

Since no data exists on the irradiation behavior of proposed GFR fuels under GFR core operating conditions, the assessments in this report are made on the basis of scoping analysis of fuel concepts. A combination of relatively simple behavior correlations and finite element analysis were used to make relative judgments about the impact of minor actinide loading on fuel burnup lifetime. It appears from literature data that the primary factor distinguishing MA-bearing fuel behavior is the generation of large additional inventories of helium gas due to capture and decay processes beginning with ^{241}Am . This large gas inventory results in increased stress on the cladding or matrix, and is particularly problematic for the GFR, where loss of core pressurization results both in a rapid temperature rise and the removal gas overpressure that acts as a restraining force. This assessment was therefore focused on the response of several fuel types to this increased gas inventory, particularly during core accident conditions.

A quantitative assessment of the limits of minor actinide content as a function of fuel burnup limit and fuel temperature limit is not currently possible. This is due to two reasons. First, fuel behavior under irradiation is extremely complex, and it is impossible at this time to take into account all parameters that affect fuel lifetime. Second, the high temperature material properties of proposed cladding and matrix materials under irradiation are not well known. Further, the fracture behavior of ceramic materials depends on fabrication process and is microstructure and geometry dependent. These issues make it imperative that fuel irradiation testing be conducted as part of a feasibility assessment.

5.1 Pin-type fuel

In general, pin-type fuel is most adaptable to the issues posed by burning minor actinides. Fuel to plenum volume ratios can be adjusted to account for the increased gas inventory at the cost of increased pressure drop across the core and a larger volume required for the core primary pressure vessel. Creep strengths of refractory metal cladding materials are quite low at GFR accident temperatures and conventional sealed pin-type fuels would require a very large plenum, perhaps on the order of 3X the fuel volume to accommodate

the gas release at an americium loading of 10 at.% of the heavy metal. The consequences of allowing fuel failure during accident conditions are not well understood. If, however, severe ballooning of the cladding occurs, flow blockage could result in an uncoolable core geometry.

An alternative to sealed pin-type fuel may be vented fuel or fuel fitted with a rupture disk system. In this case, considering only gas-loading of the cladding as the life-limiting factor for the fuel, the potential for MA loading is much higher, and there are no requirements for a long gas plenum. In the case of vented fuel, pin external and internal pressures are approximately in equilibrium, resulting in very low cladding hoop stress and no propensity toward cladding creep. Fission product release from the pins to the coolant is controlled by using a filter or series of porous carbon and/or metal frit filters. Use of a vented fuel adds considerable complexity to the GRF in terms of core design and fuel handling.

In the case of fuel that vents through a rupture disk, fission products are released to the coolant only during accidents where pin internal pressure rises beyond the limits of the rupture disk. This would prevent potential flow blockage issues due to ‘ballooning’ of the cladding from arising during accident conditions. Use of this concept would likely result in a decrease in fuel reliability during normal operating conditions.

Given a fuel to plenum ratio typical of fast reactors in the range of 1.2:1 – 1.5:1, incorporation of americium at levels beyond approximately 5 at.% into conventional sealed pin-type fuels results in a significantly higher risk of fuel failure during core accident conditions. The consequences of this failure may be high if excessive fuel diametral strain results in flow blockage within the core.

Vented concepts for pin-type fuels (both open pins and rupture disks) pose no real limitations with regard to the impact of minor actinide inventory on gas pressure driven cladding stress on fuel behavior during failure. Fuel lifetime limitations are not typical of conventional sodium-cooled fast reactors or water-cooled reactors, and are not well understood. Allowable minor actinide loading in this case could almost certainly be such that more than 20% americium could be incorporated in the fuel.

5.2 Particle bed fuel

Because particle packing density is low and all fission gas must be accommodated internally in a ‘buffer layer’ (effectively a gas plenum), fuel particle coating layers must be very thin relative to those used on TRISO fuel. As a result, high stresses are generated in the fuel particle shell wall under core accident conditions even for fuels containing no americium. As with all GFR fuel concepts, the lack of strength data for chemically vapor deposited titanium nitride (CVD-TiN) prevents a quantitative assessment of failure probability under these conditions. Typical strengths for monolithic nitride ceramic materials are on the order of 400-600 MPa, however. If a ‘factor of safety’ of 5X less than fracture stress under accident conditions is applied (100 MPa peak stress at 1600°C), then it is clear that this concept is marginal at the target burnup level of 10 at.-%

without the incorporation of americium. Incorporation of Am further decreases the probability that this fuel concept will perform adequately.

5.3 Dispersion fuel

Because of the nature of dispersion fuel, the 'gas plenum' is integral to the fuel particle. Increase in 'gas plenum' volume always result in lower heavy metal density in the fuel. This is in contrast to pin-type fuels, where increasing the gas plenum length has no impact on the heavy metal density within the GFR active core volume. Dispersion fuel thus offers less flexibility than pin-type fuel for burning minor actinides whose primary fuel performance attribute is the generation of additional gas inventory.

Because of the complex microstructure of dispersion fuels, two separate finite element models are required to gauge fuel performance. A macroscopic model with no microstructural detail is used to calculate macroscopic thermal stresses and fuel temperatures. A micro-scale model was used to calculate the local stress state of the fuel element due to gas pressure and fuel particle swelling as a function of americium content. Fuel to coolant ratio was kept constant at 50 vol.% for all concepts. Fuel particle loading was also fixed at 50 vol.%.

Some further evolution of macroscopic dispersion fuel design is required. Models incorporating all of the features of a hexagonal block type element indicate high stresses at the corners of the blocks that must be reduced. Smaller diameter high aspect ratio elements bundled into a fuel assembly offer a potential alternative design that operate at a lower temperature, lower temperature gradient, and consequently a much lower internal stress level. Dispersion fuel models indicate a significant increase in matrix stress at americium levels above approximately 5 at.% during core accident conditions, where temperatures are assumed to be reach 1600°C. The increase in gas inventory would likely result in lower design burnup limits for the fuel based on the levels of matrix stress achieved during these conditions. At 5 at.% Am content, burnup limits determined on the basis of core accident behavior can be expected to be approximately 1-2% lower than for a fuel containing no americium. Dispersion fuel is thus considered a viable concept for managing minor actinides at levels on the order of 5 at.% heavy metal or less.

5.4 Conclusions related to further modeling of GFR fuel

The assessments in this report on the feasibility of using GFR fuel for MA burning are made on the basis of scoping analysis of fuel concepts; little experimental data is available to support these assessments. Some further incremental progress on determining the viability of minor actinide transmutation using GFR fuel concepts can be made by developing more sophisticated fuel performance models; this also requires that a well defined set of material properties and irradiation performance correlations be available for use by fuel designers and modelers. In addition, analysis of the potential effects of the shift in fission product distribution on internal fuel chemistry can be more clearly defined, as well as potential decreases in fuel thermal conductivity. In the end, due to the extremely complex nature of fuel behavior under irradiation, fuel irradiation

testing is necessary for final determination of viability; without irradiation test data, no concrete statements about viability can be made. This is especially true for the GFR, where operating parameters and fuel physical requirements are outside of the envelope of the current experimental fuel database.

6. REFERENCES

- [1] L.L. Snead, J.W. Klett, "Ceramic Composites for Structural Applications," *Proc. GLOBAL 2003*, American Nuclear Society (2003) 1077-1078.
- [2] see for example B.J. Makenas, J. W. Hales, A.L. Ward, "Fuels Irradiation Testing for the SP-100 Program," *Proc. 8th Symposium on Space Nuclear Power Systems*, AIP (1991) 886-891.
- [3] E.A. Hofman, T.A. Taiwo, "Physics Studies of Preliminary Gas-Cooled Fast Reactor Designs," *Proc. GLOBAL 2003*, American Nuclear Society (2003) 82-91.
- [4] Gamma Engineering Proposal to DOE for FY-2003 SBIR Phase 1 Solicitation, "Development of a Hybrid SiC/SiC Ceramic Composite for Gas Cooled Fast Reactor Fuel Cladding and Core Structural," January, 2003.
- [5] D. Smith, P. McIntyre, B. Basaran, M. Yavuz, "SiC Composite: A New Fuel Cladding for High-Temperature Cores," *Proc. GLOBAL 2003*, American Nuclear Society (2003) 1821-1823.
- [6] S.J. Zinkle, "Nonfissile Ceramics for Future Nuclear Systems," *Proc. GLOBAL 2003*, American Nuclear Society (2003) 1066-1067.
- [7] L.P. Hatch, W.H. Regan, J.R. Powell, "Fluidized Bed for Rocket Propulsion," *Nucleonics* 18 [12] (1960) 102.
- [8] A.C. Marshall, "A Review of Gas-Cooled Reactor Concepts for SDI Applications," Sandia report SAND-87-0558 (1989).
- [9] J.R. Powell, H. Ludewig, F.L. Horn, K. Araj, R. Benenati, O. Lazareth, G. Slovik, M. Solon, W. Tappe, J. Belisle, B. Short, R. DeMars, C. Caldwell, W. Pettus, R. Zavadowski, R. Boyle, A. Pietsch, "Nuclear Propulsion Systems for Orbit Transfer based on the Particle Bed Reactor," *Space Nuclear Power Systems 1988*, Eds. M.S. El-Genk, M.D. Hoover, Orbit Book Company, Malabar, FL (1989) 185-198.
- [10] H. Ludewig, J.R. Powell, M. Todosow, G. Maise, R. Barletta, D.G. Schweitzer, "Design of Particle Bed Reactors for the Space Nuclear Thermal Propulsion Program," *Prog. Nucl. Energy*, Vol. 30, No. 1 (1996) 1-65.
- [11] M. Konomura, T. Saigusa, T. Mizuno, Y. Ohkubo, "A Promising Gas-Cooled Reactor Concept and its R&D Plan," *Proc. GLOBAL 2003*, American Nuclear Society (2003) 57-64.
- [12] INERI GFR Project CEA/ANL Technical Workshop, Cadarache, France October (2002).
- [13] Weber, C. E. and Hirsch, H. H., "Dispersion-Type Fuel Elements", *International Conference on the Peaceful Uses of Atomic Energy, Geneva, Switzerland*, P/561 (1955).
- [14] Weber, C. E., "Progress on Dispersion Elements", *Progress in Nuclear Energy Series V: Metallurgy and Fuels*, 2 295-362 (1959).
- [15] see for example, J.D.B. Lambert, "Irradiation Study of UO₂-Stainless Steel and (Pu,U)O₂ -Stainless Steel Cermet Fuels in Rod and Plate Geometry," p. 237-254 in *High*

Temperature Nuclear Fuels, Metallurgical Society Conference Vol. 42, ed. A.N. Holden, Gordon and Breach (1966).

[16] D.L. Keller, G.W. Cunningham, W.E. Murr, E.O. Fromm, D.E. Lozier, "High-Temperature Irradiation Test of UO₂ Cermet Fuels," report BMI-1608 (1963).

[17] W.C. Thurber, F.R. McQuilkin, E.L. Long, M.F. Osborne, "Irradiation Testing of Fuel for Core B of the Enrico Fermi Fast Breeder Reactor," report ORNL-3709 (1964).

[18] Neeft, E.A.C., Bakker, K., Schram, R.P.C., Conrad, R., Konings, R.J.M., "The EFTTRA-T3 Irradiation Experiment on Inert Matrix Fuels," *J. Nucl. Mater.* **320** (2003) 106-116.

[19] Georgenthum, V., Chauvin, N., Pelletier, M., Noitor, J., Berlanga, C., Brenet, D., "Influence of the Microstructure for Inert Matrix Fuel Behaviour: Experimental Results and Calculations," Proceedings of the GLOBAL 99 International Conference on Future Nuclear Systems, Jackson Hole, WY USA August 29-September 3, (1999).

[20] Nitani, N., et al., "In-pile irradiation of rock-like oxide fuels", *J. Nucl. Mater.* **319** (2003) 102.

[21] Noirot, J., Desgranges, L., Chauvin, N., Georgenthum, V., "Postirradiation Examinations of THERMHET Composites Fuels for Transmutation," *J. Nucl. Mater.* **320** (2003) 117-125.

[22] R.A. Lowden, J.C. McLaughlin, J.R. Kelley, "Nitride Ceramic Coatings for Gas-Cooled Fast Reactor Particle Fuel," *Proc. GLOBAL 2003*, American Nuclear Society (2003) 523-524.

[23] Minato, K., Ogawa, T., Fukuda, K., Sekino, H., Kitagawa, I., Mita, Naoaki, "Fission Product Release from ZrC-coated Fuel Particles During Postirradiation Heating at 1800 and 2000°C," *J. Nucl. Mater.* **249** (1997) 142-149.

[24] For a comprehensive review of the state of the art with respect to coated particle fuels circa. 1977 see, *Nucl. Tech.* **35**, No. 2 (1977).

[25] Kurina, I.S., Moseev, L.I., "Fabrication and Study of the Properties of PuO₂-MgO," *Atomnaya Energiya* vol. 82, No. 5 (1997) 355-358.

[26] Fernandez, A., Konings, R.J.M., Somers, J., "Design and Fabrication of Specific Ceramic-Metallic Fuels and Targets," *J. Nucl. Mater.* **319** (2003) 44-50.

[27] Proceedings of the 8th Inert Matrix Fuel Workshop (IMF-8), *J. Nucl. Mater.* **319** (2003) 1-187.

[28] Proceedings of the 2nd Seminar on European Research on Materials for Transmutation, *J. Nucl. Mater.* **320** (2003) 1-176.

[29] INERI GFR Project CEA/ANL Technical Workshop, Cadarache, France, March (2003).

[30] S. Pillon, N. Schmidt, E. Abonneau, Y. Croixmarie, L. Donnet, S. Hayes, M. Meyer, K. Chidester, B. Margevicius, A. Fernandez, D. Hass, "The FUTURIX-FTA Experiment in Phenix," *Proc. GLOBAL 2003*, American Nuclear Society (2003) 220-227.

[31] Nitani, N., et al., "In-pile irradiation of rock-like oxide fuels", *J. Nucl. Mater.* **319** (2003) 102.

[32] S.J. Zinkle, "Nonfissile Ceramics for Future Nuclear Systems," *Proc. GLOBAL 2003*, American Nuclear Society (2003) 1066-1067.

[33] R.O. Elliot, C.P. Kempter, *J. Phys. Chem.*, **62** (1958) 630.

-
- [34] P. Barnier, C. Brodhag, F. Thevenot, "Hot-Pressing Kinetics of Zirconium Carbide," *J. Mater. Sci.* 21 (1986) 2547-2552.
- [35] T. Ya. Kosolapova, *Carbides: Properties, Production, and Applications*, Plenum Press, NY (1971).
- [36] *Modern Ceramics*, ed. J.E. Hove and W.C. Riley, John Wiley & Sons, New York (1965) 338.
- [37] T. Ya. Kosolapova, *Carbides: Properties, Production, and Applications*, Plenum Press, NY (1971) 26-27.
- [38] P. Patriarca, D.J. Rucker, *Fuels and Materials Development Program Quarterly Progress Report for Period Ending September 30, 1969*, ORNL-4480 (1970).
- [39] *see for example*, Minato, K., Ogawa, T., Koya, T., Sekino, H., Tomita, T., "Retention of Fission Product Caesium in ZrC-coated Fuel Particles for High-Temperature Gas-Cooled Reactors," *J. Nucl. Mater.* 279 (2000) 181-188.
- [40] Minato, K., Ogawa, T., Fukuda, K., Sekino, H., Kitagawa, I., Mita, Naoaki, "Fission Product Release from ZrC-coated Fuel Particles During Postirradiation Heating at 1800 and 2000°C," *J. Nucl. Mater.* 249 (1997) 142-149.
- [41] E.G. Kendall, "The Development and Evaluation of Hypereutectic Carbides," in *Modern Ceramics*, ed. J.E. Hove and W.C. Riley, John Wiley & Sons, New York (1965).
- [42] Hojou, K.; Otsu, H.; Furuno, S.; Izui, K.; Tsukamoto, T. , "In-situ Observation of Damage Evolution in Titanium Carbide Crystals During Helium Ion Irradiation," *J. Nucl. Mater.* 212-215 (1994) 281-286.
- [43] Iseki, M.; Kabeya, Z, "Surface Erosion of Substoichiometric Titanium Carbide under High Energy 4He+ Ion Bombardment," *J. Nucl. Mater.* 133-134 (1985) 722-726.
- [44] H. Mostaghaci, *Applications of Advanced Materials in a High Tech Society I - Advanced Ceramic Materials*, Trans Tech publications Ltd., Switzerland (1996).
- [45] Brooks, R., J., *Concise Encyclopedia of Advanced Ceramic Materials*, MIT Press Cambridge Massachusetts (1991).
- [46] M. Rohde, B. Schulz, ASTM-STP-1125 (1992) 764.
- [47] *Engineering Materials Handbook Vol. 4 Ceramics and Glasses*, ASM International, Metals Park Ohio (1991).
- [48] Yano, Toyohiko; Iseki, Takayoshi , "Swelling and Microstructure of Aluminum Nitride Irradiated in a Fast Reactor," *J. Nucl. Mater.* 203 (1993) 249-254.
- [49] Yano, Toyohiko; Iseki, Takayoshi, "Thermal and Mechanical Properties of Neutron-Irradiated Aluminum Nitride," *J. Nucl. Mater.* 179-181 (1991) 387-390.
- [50] J.E. Hove, W.C. Riley, *Modern Ceramics*, John Wiley & Sons, New York (1965) 354.
- [51] Chauvin, N., Albiol, T., Mazoyer, R., Noiroot, J., Lespiaux, D., Dumas, J.C., Weinberg, C., Menard, J.C., Ottaviani, J.P., "In-pile Studies of Inert Matrices with Emphasis on Magnesia and Magnesium Aluminate Spinel," *J. Nucl. Mater.* 274 (1999) 91-97.
- [52] R. Thetford, M. Mignanelli. "The Chemistry and Physics of Modelling nitride Fuels for Transmutation," *J. Nucl. Mater.* 320 (2003) 44-53.
- [53] Arai, Y., Iwai, T., Nakajima, K., Shirai, O., Kikuchi, H., Amezawa, H., Hayashi, H., Minato, K., "Proc. 7th OECD/NEA Information Exchange Meeting on Actinide and Fission Product Partitioning and Transmutation, Jeju, ROK, 14-16 October 2002.

-
- [54] Streit, M., Ingold, F., Pouchon, M., Gauckler, L.J., Ottaviani, J.-P., "Zirconium Nitride as Inert Matrix for Fast Systems," *J. Nucl. Mater.* 319 (2003) 51-58.
- [55] see for example B.J. Makena, J. W. Hales, A.L. Ward, "Fuels Irradiation Testing for the SP-100 Program," Proc. 8th Symposium on Space Nuclear Power Systems, AIP (1991) 886-891.
- [56] T.E. Tietz and J.W. Wilson, Behavior and Properties of Refractory Metals, Stanford University Press (1965).
- [57] D.J. Senior, J. K. Thomas, K.L. Peddicord, "Thermophysical Property Correlations for the Niobium-1% Zirconium Alloy," and "Transport Property Correlations for the Niobium-1% Zirconium Alloy," *J. Nucl. Mater.* 173 (1990) 261-283
- [58] F.W. Wiffen, Effects of Irradiation on Properties of Refractory Alloys with Emphasis on Space Power Reactor Applications," p. 252-277 in *Refractory Alloy Technology for Space Nuclear Power Applications*, ed. R.H. Cooper, E.E. Hoffman OSTI report CONF-8308130 (1984).
- [59] see for example E.E. Hucke, U.S. Patent 3,859,421, "Methods of Producing Carbonaceous Bodies and the Products Thereof," Jan. 7, 1975.
- [60] J.V. Shennan, "Dispersed Ceramic Fuels for the Advanced Gas-Cooled Reactor," p. 96-110 in Preparation of Nuclear Fuels, Nuclear Engineering Part XVIII, eds. A.D. Tevebaugh and D.L. Keller, Chemical Engineering Progress Symposium Series No. 80, Vol. 63 (1967).
- [61] D.L. Keller, G.W. Cunningham, W.E. Murr, E.O. Fromm, D.E. Lozier, "High-Temperature Irradiation Test of UO₂ Cermet Fuels," report BMI-1608 (1963).
- [62] R.J.M. Konings, et al., *J. Nuc. Mat.* 282 (2000) 159-170.
- [63] Storms, E. K., "An Equation which Describes Fission Gas Release from UN Reactor Fuel," *Journal of Nuclear Materials* **158** 119-129 (1988).
- [64] Timoshenko, S. P. and Goodier, J. N., *Theory of Elasticity*, McGraw-Hill, Inc. (1970).